CHAPTER 5

MAGNETIC SURVEY

Chapter 5. Magnetic Survey

5–1 Purpose of Survey

Because of the strong correlation observed between geothermics and igneous activity, the distribution and shape of igneous rocks, which has a close relation with geothermal fluids, can be determined by observing the geomagnetic field.

The magnetic method depends upon measuring accurately the anomalies of the local geomagnetic field produced by the variations in the intensity of magnetization in rock formations.

The magnetization of rocks is partly due to induction by the magnetizing force associated with the earth's field and partly to their remanent magnetization.
The induced intensity depends primarily upon the magnetic susceptibility as well as the magnetizing force, and the permanent intensity upon the geological history of the rock.
Research in the permanent intensity of rocks, especially since 1950, has given rise to the subject of palaeomagnetism.

Around the geothermal field where high temperature geothermal fluids might exist at depths, positive magnetic anomaly is a unique phenomenon due to the demagnetizing effect.

In this survey, presumption of underground structures by the slight change of magnetic intensity and consideration on geothermal structure are planned to be discussed with use of the high sensitive magnetometer.

5–2 Method of Survey

5–2–1 Abstract

The earth's magnetic field resembles the field of a large bar magnetic near its center or that due to a uniformly magnetized sphere.
The direction of the field is vertical at the north and south magnetic poles, and horizontal at the magnetic equator.
The intensity of the field, which is a function of the density of the 'flux lines' shown below, again behaves as a bar magnet being twice as large in the polar region as in the equatorial region, or appoximately 60,000 γ (gammas) in Northern Canada and less than 30,000 γ in middle South America respectively.
The total intensity is shown in Fig. II–5–1.
The earth cannot exactly be represented by a single bar magnet, but has numerous higher order poles and very large-scale anomalous features owing to unknown characteristics of the generating mechanism in the earth's core.
But for the purpose of this survey, most relevant deviation from a standard field is the anomalous set of features in the ground caused by local variations in the magnetic minerals or other features

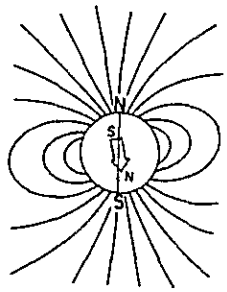

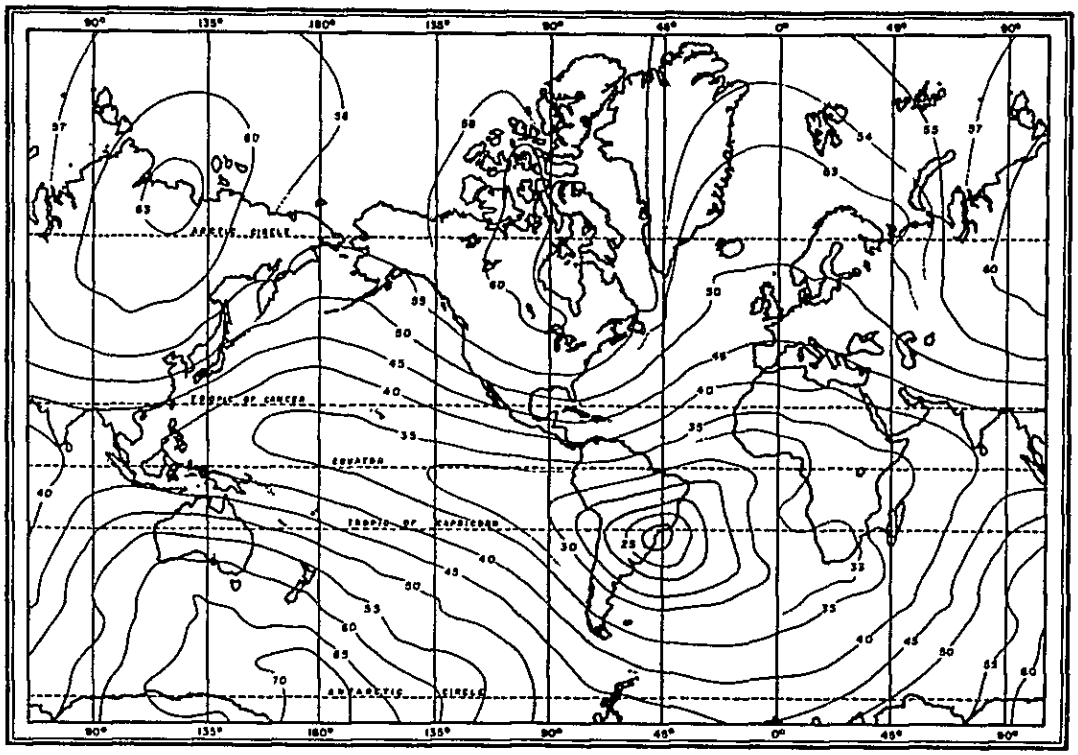

Fig. II–5–1 Total Intensity of the Geomagnetic Field

of interest which distort the local earth's magnetic field.

As mentioned above the magnetization of rocks is partly due to induction by the magnetizing force associated with the earth's field and partly to their remanent magnetization.

Induced magnetization is proportional to the intensity of magnetic field and the susceptibility of rocks.

The induced magnetization is equal to the product of the volume magnetic susceptibility, k, and the earth's or ambient field intensity, F, or

$$Ii = kF$$

where Ii is the induced magnetization per unit volume in CGS electromagnetic units and F is the field intensity in Gauss ($G=10^{-5}\ \gamma$). The susceptibility of rocks is almost entirely controlled by the amount of magnetite in them.

Other than magnetite, some minerals also show magnetism, but magnetite is the most popular mineral and the relation between weight percentage ρ and susceptibility k will be as follows,

$$k = 0.3\ \rho$$

Typical susceptibilities of rocks are given below, but may vary by an order of magnitude or more in most cases:

Altered ultra basic rocks	10^{-4} – 10^{-2}
Basalt	10^{-4} – 10^{-3}
Gabbro	10^{-4}
Granite	10^{-5} – 10^{-3}
Andesite	10^{-4}
Rhyolite	10^{-5} – 10^{-4}
Metamorphic rocks	10^{-4} – 10^{-6}
Sedimentary rocks	10^{-6} – 10^{-5}
Limestone-chert	10^{-6}

Typically, dark, more basic igneous rocks possess a higher susceptibility than the acid igneous rocks and the latter, in turn, higher than sedimentary rocks.

The remanent magnetization of a rock or object may or may not be in the same direction as the present earth's field for the object may be reoriented because the earth's field is known to have changed its orientation in geological and even historic time. The direction of remanent magnetization is not constant, but it does not effect so much the magnetic structure interpretation.

• Total Field Measurement

The total magnetic field intensity, as measured by a proton magnetometer, is a scalar measurement, or simply the magnitude of the earth's field vector independent of its direction.

Total field intensity is very significant with respeet to the asymmetric signatures of anomalies, interpretation of anomalies, and in various special applications.

The depth, shape and the susceptibility difference can be determined by the shape of anomaly, amplitude and wavelength.

Anomalies of very short wavelengths are presently caused by the magnetic effects of operator, or simply by surface magnetization contrasts in the surface or near-surface materials.

A 5point running average was adopted on each observed value for every 50m interval. The average values are then plotted on the plain and section maps.

5–2–2 Survey Line and Station

The area with the most intense values in this survey lies between Puchuldiza and Tuja with Mt. Tahipicollo as its center. Thus, 14 lines measuring 4,000 m each were planned to cross the area in N–S direction.

The line interval is in principle 500m, but some additional lines were planned between survey lines in Tuja area and along the Puchuldiza creek by the road.

The length of the line is 4,000m for a coordinate of 858N to 854N, and for Line-11 and Line-12, 1,000m more were extended towards the south in order to investigate the Puchuldiza manifestations. Direction of the survey line was checked by confirming the gravity stations.

Line–1 is along 499.5E and Line 14 along 506E. Location map of survey lines are shown on Fig. II–5–2. Station interval is 50m numbering 0 – 80 from north to south. Total observation stations numbered 1300.

5–2–3 Magnetometer

Proton magnetometer used are as follows,

Specification

Portable proton magnetometer G–816 made by Geometrics, Inc., U.S.A.

Resolution. . . . ± 1 gamma throughout tuning range

Tuning Range . . . . 20,000 to 90,000 γ (world-wide)

Gradient Tolerance . . . . 150 gamma/foot

Size and Weight . . . .

Console	9.5 x 18 x 27cm	2.5kg
Sensor	11cm dia x 15cm	
Staff	3.0cm dia x 244cm	

Theory

It has been some time since the nuclear magnetic resonance (NMR) type of magnetometer was used to measure the geomagnetic field. In recent years, the measuring instruments have been widely used in rugged topography with efficiency due to miniaturization and digital read-out system.

The nuclear magnetic resonance type magnetometer utilizes the magnetic gyration characteristics of the hydrogen nucleus (proton). By measuring the frequency of free precession of the proton in the geomagnetic field, it is possible to measure the strength of the geomagnetic field.

As the proton is in existence abundant in water, kerosene and alcohol, these liquids may be sealed in a container surrounded by a coil (pick up and polarizing coil). When momentarily the polarizing field stronger than geomagnetic field is applied, the protons will line up in the direction of the polarizing field. And when the polarizing field is suddenly cut off, the protons will process like a spinning top about the direction of the geomagnetic field.
In this case the free-precession frequency, f, is proportional to the geomagnetic field strength Ho, so that

$$Ho = 2\pi f/\gamma$$

In the above equation, γ is called the gyromagnetic ratio (magnetic moment/spin angular momentum) of the proton. It is a physical constant depending on the types of nuclei and its value for the proton is 0.26752.

In the abovementioned manner, by using the same polarizing coil, it is possible to measure the frequency, which is proportionate to the strength of the geomagnetic field.

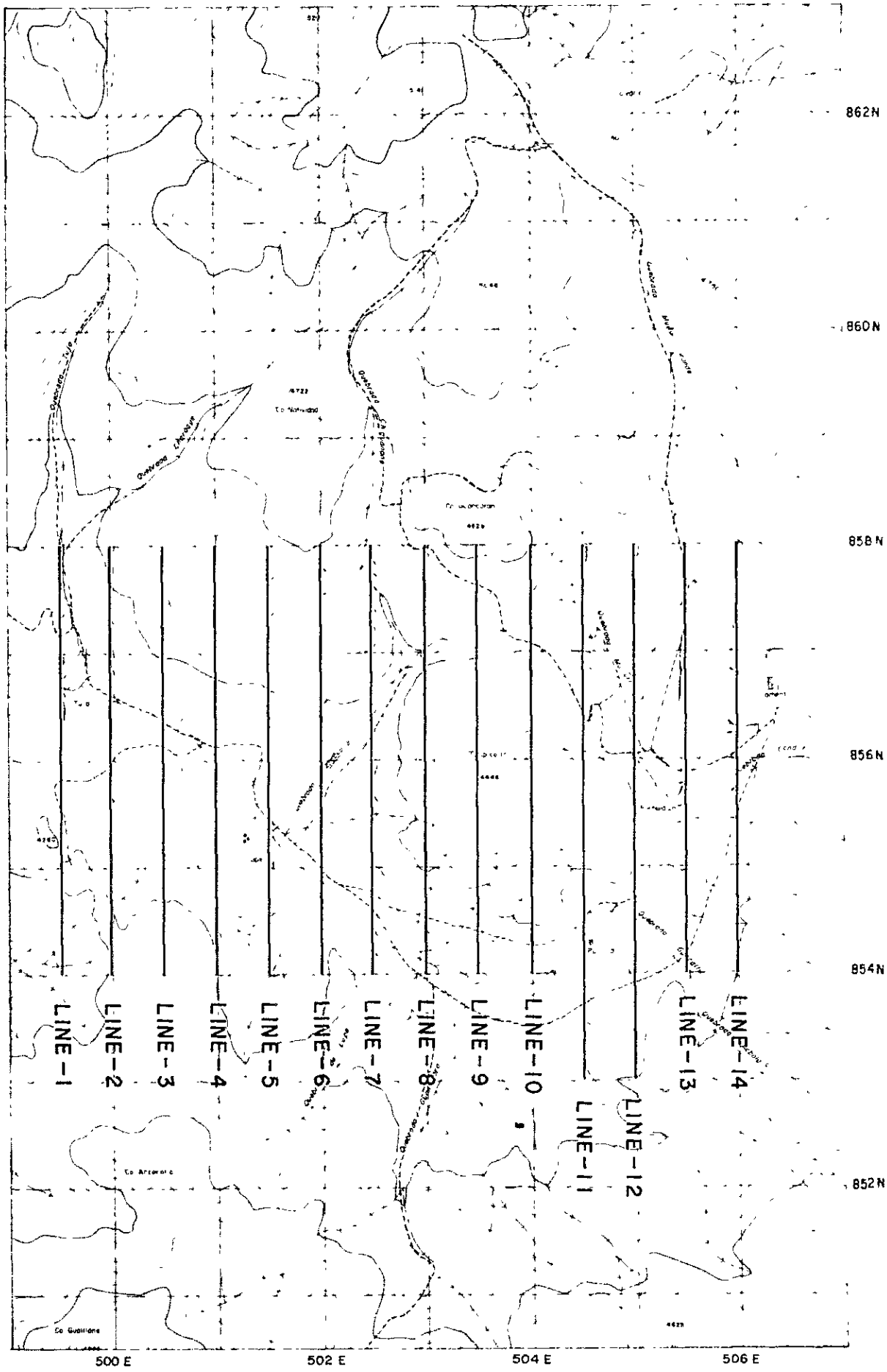

Fig Ⅱ-5-2

LOCATION OF MAGNETIC SURVEY LINES

5–2–4 Magnetic Correction

The variation described above all refer to the spacial variations in the earth's magnetic field, but there are variations in time as well.

Significant time variations with periods of seconds, minutes and hours are the direct or indirect effect of the solar wind as it distorts the magnetosphere or external magnetic field.

For very important field measurements, particularly for higher resolution measurements, a recording base station or reference monitor is examined at the start of each day and after every use for an indication of magnetic storm activity and also for subsequent diurnal variations from field data using time as a correlation (Fig. II–5–3).

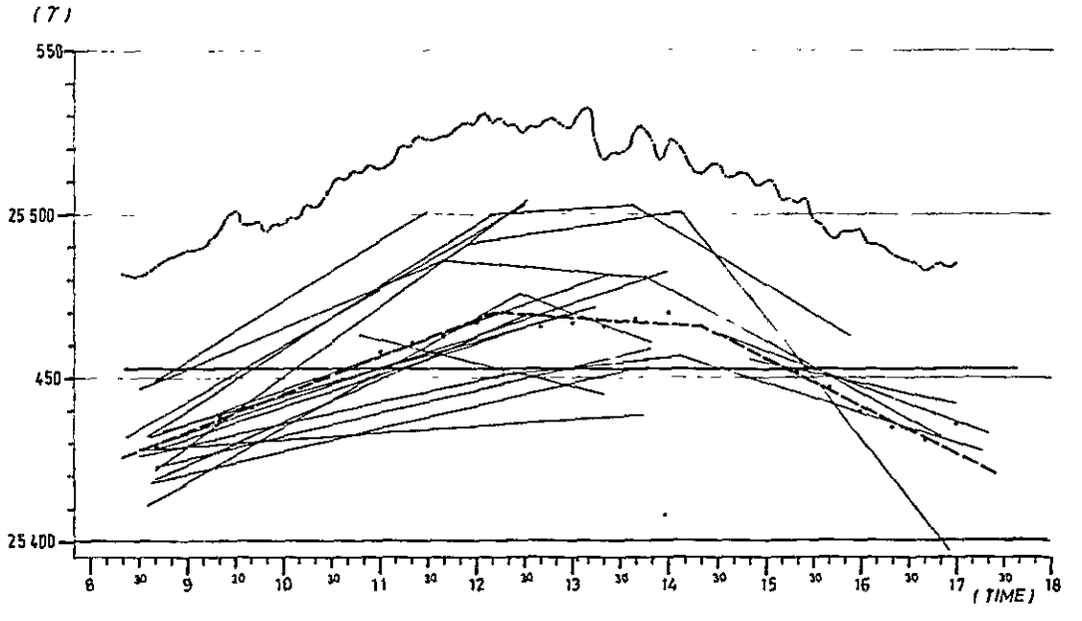

Fig. II–5–3 Diurnal Variation at Magnetic Station

In this survey only one magnetometer was used, so the following diurnal variation correction was adopted in order to compensate the error as much as possible.

As seen on above magnetic change, magnetic intensity increase monotonously in the morning, little change at noon time and decrease monotonously in the afternoon.

Magnetic variation on the base point was made by four observations every day: in the morning before starting, the end of morning observation, noon before starting and the end of observation in the evening.

Magnetic change is approximated by three straight lines after averaging 10 minutes interval. The correction values are obtained as the difference between those lines and the average of all the data of the base point (25,453 γ) and are time allotted on every observed value.

Correction value $\Delta\gamma t$ were obtained by the following formula,

$$\Delta\gamma t = \begin{cases} 11.5t - 123 & t \leq 12.2 \\ -2t + 41.5 & 12.2 < t \leq 14.33 \\ -14.5t + 221 & 14.33 < t \end{cases}$$

where, t is the time of observation and when corrected value and observed value are γ c and γo, respectively, the correction becomes

$$\gamma c = \gamma o - \Delta\gamma t$$

As observed magnetic intensity contains geological noises near surface and short wave anomalies due to micropulsation, the average of 5 measurements γs are calculated to know the deep magnetic anomaly.

$$\gamma s = \frac{1}{5} \sum_{i=1}^{5} \gamma_i$$

After those corrections magnetic profile on each line are shown on Fig. II–5–4.

5–3 Method of Analysis

5–3–1 Susceptibility Measurement

In order to analyse the magnetic structure which causes the anomaly, magnetic susceptibility, the depth and the shape should be determined. Collected rock samples were measured by the following procedure.

Special care has been taken to avoid iron particles of the hammer and the mortar from mixing with the samples and an agate mortar was used to grind the samples down to –80 mesh. Sixty grams of power sample was put into a plastic tubular container (1 "Dia. x 3 "Long) and measured by the Bison 3101 System for magnetic susceptibility.

The results of the measurements are shown in Table II–5–1.

5–3–2 Cross-Section Analysis

Since the measurement in magnetic survey is a potential quantity, an indefinite number of models of magnetic rocks can give a reasonable explanation to the results of the measurement. It is therefore, necessary to determine which particular model is most appropriate to the geological structure present in the surveyed area.

Quantitative interpretation of magnetic anomalies is usually done simply with models of magnetic rocks of sphere, cylinder, prism, step or dyke structure or some combination of them.

In this case of survey, where the magnetic measurement were carried out on the surface, the obtained iso-gamma map is dominated with short wavelength anomalies due to topography of the area and magnetic rocks distributed near the surface. Running average method was applied to eliminate short wavelength anomalies of this type before quantitative interpretation of underground structure is undertaken.

Table Ⅱ-5-1 Magnetic Susceptibility

Sample No.	Period	Formation	Rock type	σ' (g/cc)	σ (g/cc)	R (Ω-m)	K ($\times 10^{-6}$ emu/cc)
1206	Quaternary		Andesite	1.92	2.51	2001	2621
1402			"	1.84	2.34	476	605
1403			"	1.84	2.53	2052	2832
3001			"	1.83	2.45	2794	3744
0101	Tertiary	Lupe F.	"	1.75	2.39	1484	2033
1205			S S	1.66	1.83	827	910
0102			Andesite	1.64	2.30	570	798
1401			"	1.87	2.55	532	713
1610		Puchuldiza	"	1.85	2.53	995	1363
2901		F.	"	1.65	2.57	1537	2398
1608			white Tf	1.49	1.99	140	188
3006		Condoriri	welded Tf	1.76	2.36	1083	1451
P3-234		F.	dacitic Tf	1.42	2.24	38	60
P4-310			"	1.48	2.26	38	58
1701		Chojna	S S	1.61	2.44	1562	2374
P5-540		Chaya F.	"	1.55	2.36	50	76
1613			Tf	1.53	2.03	15	20
1702			Lava	1.66	2.29	1324	1827
1705			white Tf	1.59	2.12	12	16
2801			and-welded Tf	1.62	2.25	75	104
2802		Utayane F.	dc-welded Tf	1.62	2.34	27	39
2803			Tf	1.61	2.04	20	25
P1-641			"	1.51	2.16	45	64
P1-697			and-Tf	1.56	2.36	76	115
P2-408			"	1.42	2.21	33	51
P2-522			"	1.37	2.34	35	60
P4-945			"	1.55	2.46	53	84
P5-1012			"	1.57	2.36	195	293
1201	Cretaceous		dc-Tf	1.54	2.30	52	78
1202		Churicollo	and-welded Tf	1.59	2.32	57	83
1203		F.	S S	1.60	2.30	40	58
2201			and-welded Tf	1.55	2.30	60	89

* P3-234 shows a sample collected at the depth of 234 m of exploratry well No.3 .

In the area of zero (degree magnetic) inclination like in this case, the result of magnetic survey is dominated with negative anomalies. And, since its contour pattern has the tendency to be elongated in east and west direction even for spherically symmetric magnetic rock, it is difficult to estimate the east and the west end of the magnetic rock which have induced the observed anomalies (Fig. II–5–5).

Normally negative anomalies are observed above high susceptibility rocks. Positive anomalies localized on the contour map or cross-section imply existence of lower susceptibility rocks which is of high interest in the case of geothermal region in relation to demagnetization phenomena.

Since (1) the measurements were carried out on the surface and the result is much affected by magnetic circumstance near the measuring point and (2) in the area of zero degree magnetic inclination, as in this case, no distinct difference is shown between pattern of magnetic anomalies of prism and those of dyke structure, for the interpretation of remarkable magnetic anomalies, curve fitting method with dyke model was performed.

Fig. II–5–6 shows the characteristics of magnetic anomaly due to dyke, horizontal cylinder and spherical model in the case of zero degree magnetic inclination.

5–4 Result of Analysis

5–4–1 Interpretation on Iso-Gamma Map (Fig. II–5–7)

Remarkable low magnetic anomalies together with high gravity anomalies mainly correspond to the distribution of the Quaternary andesitic rocks. At the north end of Line–2, at the south end and near measuring point 15 of Line–3 and Line–4, and near the north end of Line–8, –11 and –12, considerably low magnetic anomalies were detected. These low magnetic anomalies are due to intensive magnetism of the Quaternary andesitic rocks of the order of 10^{-3} magnetic susceptibility as measured from rock samples.

A weak but still well distinct low magnetic anomaly was observed near well No. 5. This was considered to have originated from the Tertiary welded tuff of Puchuldiza Formation.

Influence of demagnetization due to thermal alteration is expected to be observed as weak high magnetic anomalies. At the south end of Line–11 across Puchuldiza geothermal area, a broad high magnetic anomaly zone is seen. Another high magnetic anomaly zone extends from Tuja to the east and near measuring point 25 on Line–2 is an especially interesting region.

The relations between magnetism of rocks and observed magnetic anomalies are shown in the magnetic interpretation map of Fig. II–5–10. In the middle of the map around Mt. Tahiphicollo, an extended high magnetic anomaly zone is seen with low magnetic susceptibility rocks. Although there are some localized high susceptibility rocks as seen on the top of the mountain, the magnetic character of this region is mainly due to deep and broad low susceptibility rocks representing an extension of demagnetization effect of geothermal alteration in the past.

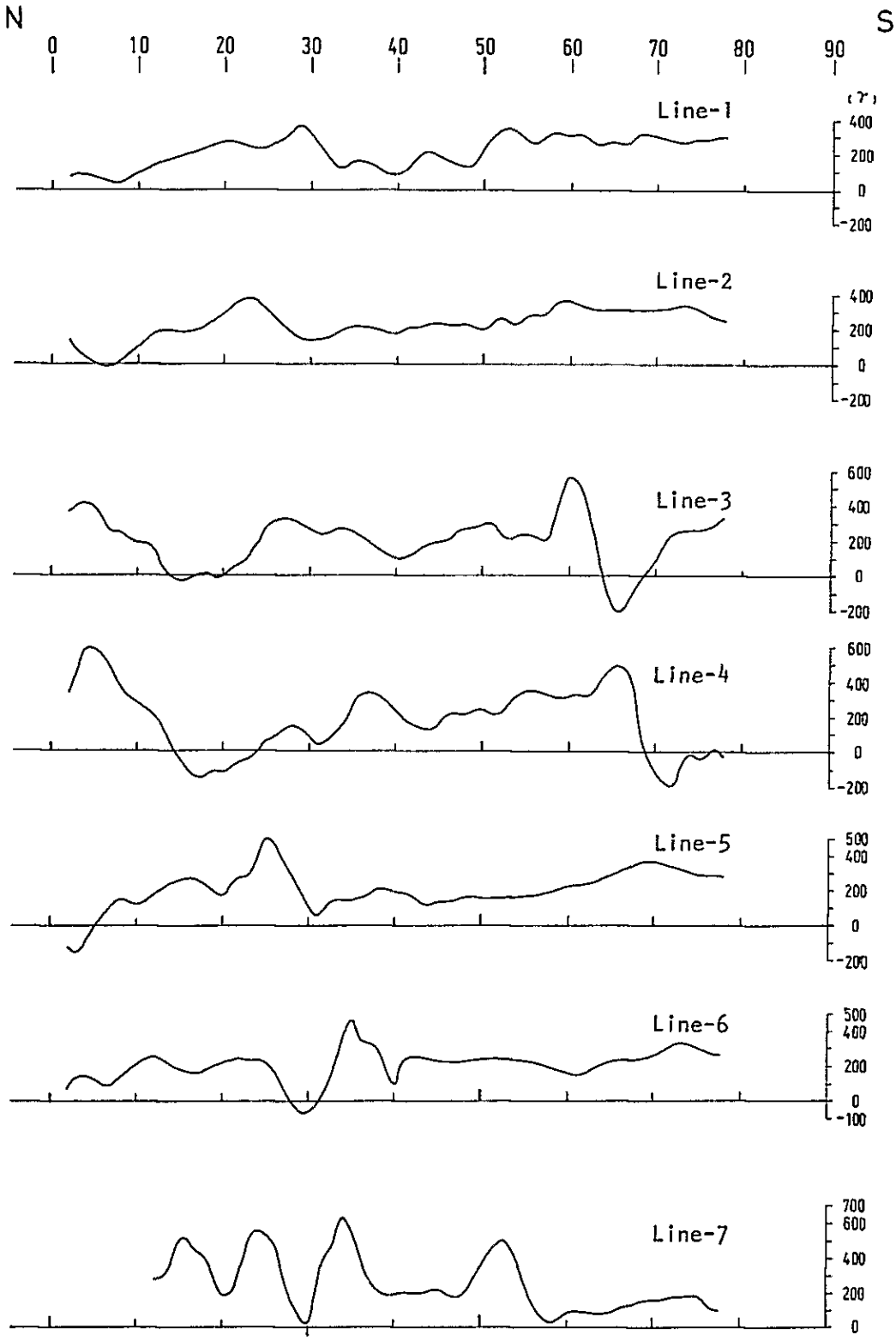

Fig. II-5-4 Magnetic profile (Line-1 - Line-7)

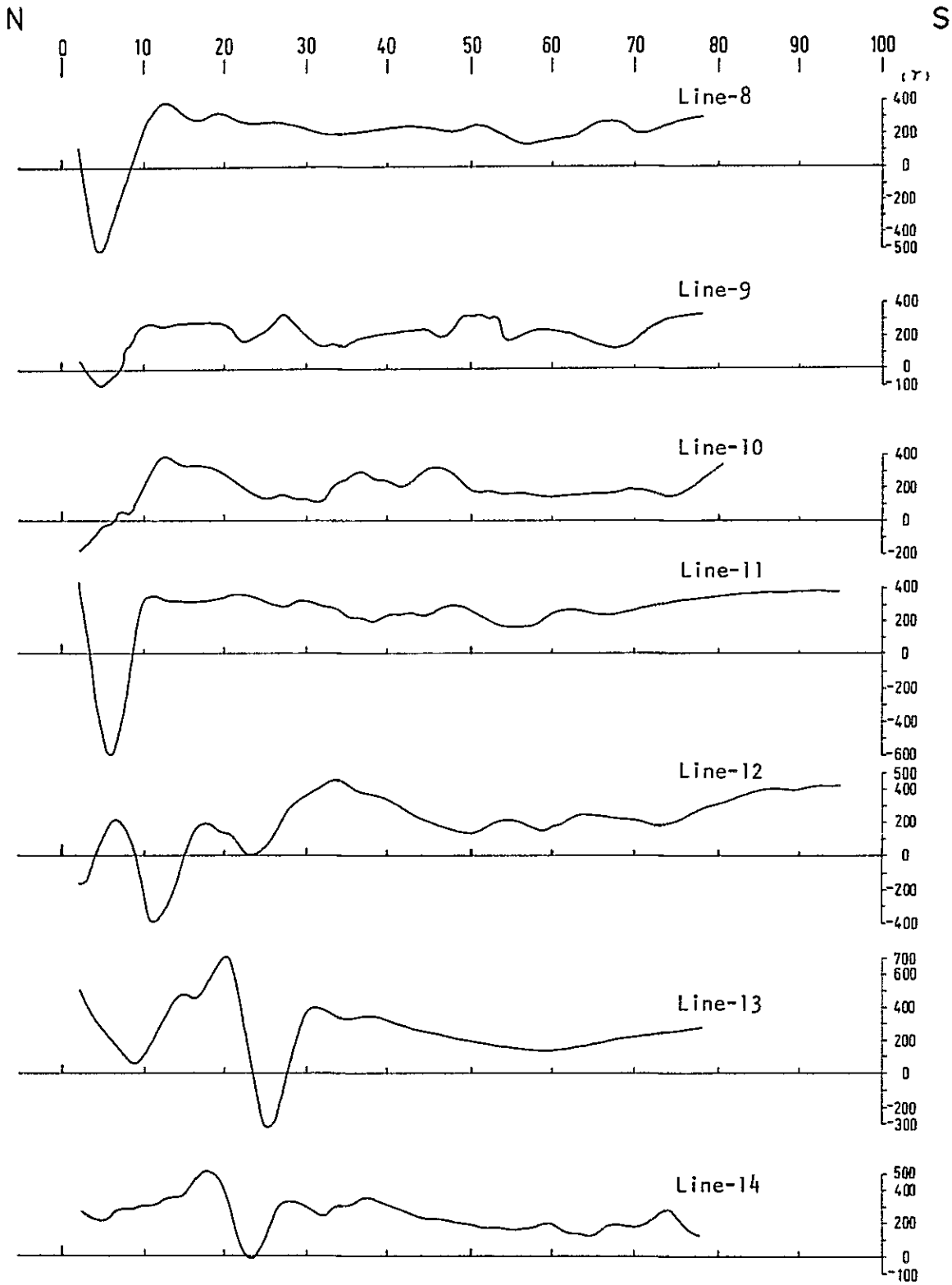

Fig. II-5-4 Magnetic profile (Line-8 - Line-14)

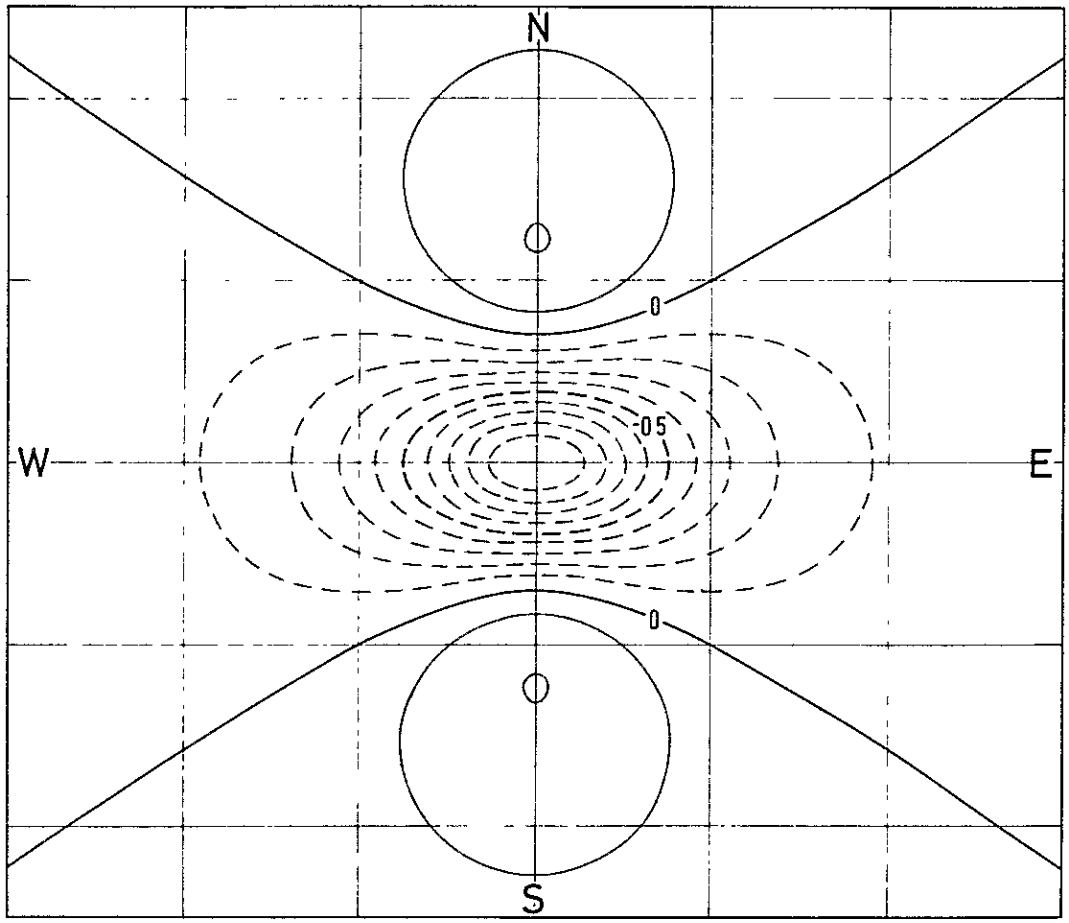

Fig. II–5–5 Magnetic Anomaly due to Sphere at the Inclination of $O^{O}N$(Radius of the sphere: 1 grid)

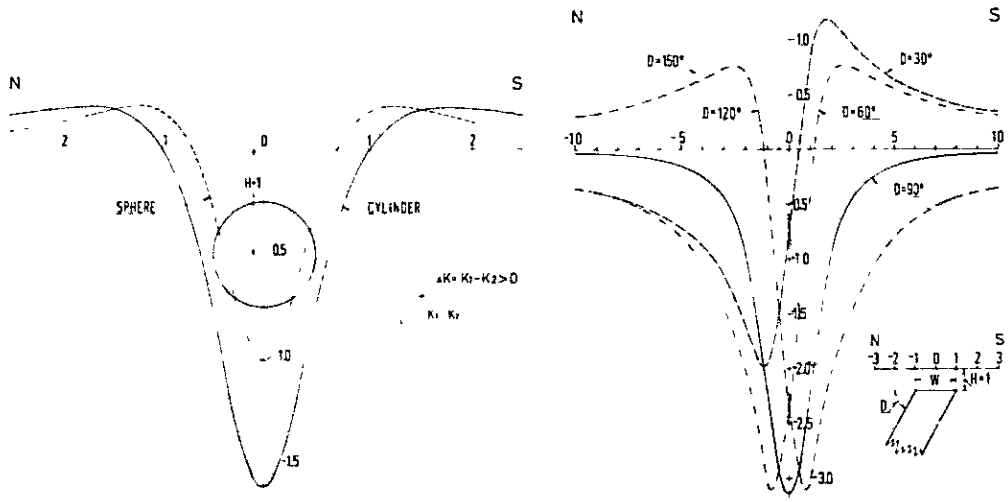

Fig. II–5–6 Magnetic Anomaly due to Sphere, Horizontal Cylinder and Dyke Models (Inclination=O^{O})

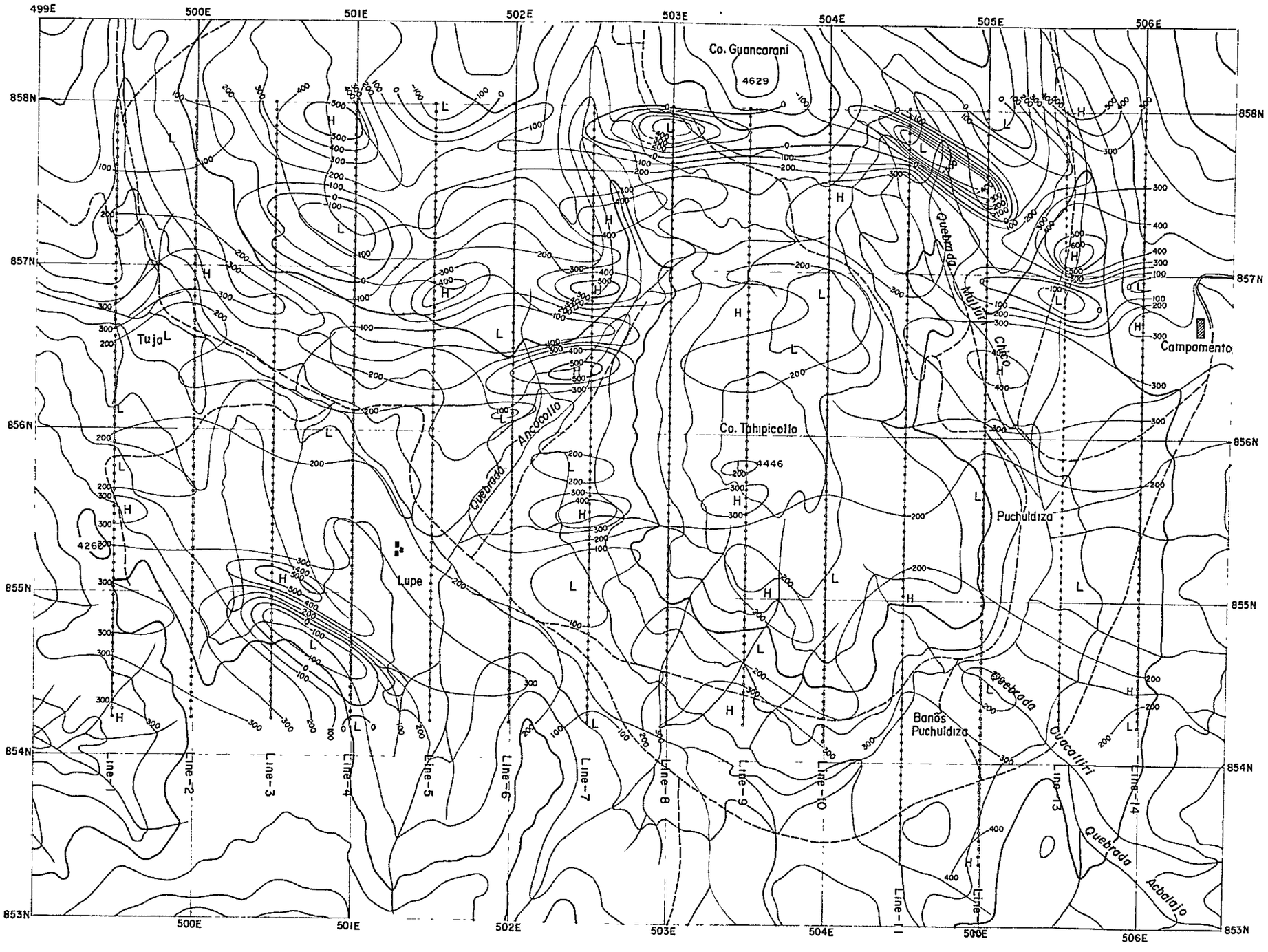

Geothermal Power Development Project
in Puchuldiza
the Republic of Chile

OBSERVED MAGNETIC MAP

1 : 25,000

0 500 1,000m

Nov~ Dec, 1978

Fig II-5-7

Analogous observations were found around Puchuldiza and the area from Tuja to the east in good accordance with present geothermal manifestations.

North of the surveyed area, around the northern part of Line A of the electrical survey, low magnetic anomaly zone due to rocks of high magnetic susceptibility was observed.
In the area north of Mt. Ancocollo on the southern part of Line–3, a low magnetic anomaly zone, where magnetic variation of over 800 γ has been detected and cross-section analysis was carried out. The procedure is briefly described as follows;

5–4–2 Interpretation of Cross-Section Analysis

A quantitative analysis was carried out with an assumed dyke structure on magnetic anomaly along the southern part of Line–3 from point No. 50 to 80 and the north end of Line–13 from point No. 10 to 40. Fig. II–5–8 shows the result of the calculation. Although this is only an example of infinite number of combinations of shape, depth and susceptibility for the assumption on the source of magnetic anomaly, the applied models of rocks are all inclined to the south with the same susceptibility around $6 - 7 \times 10^{-3}$ emu/cc which is in good agreement with the high susceptibility of the Quaternary andesitic rocks observed in rock samples as shown in Tab. II–5–1.

The following formulas were applied in the calculation of magnetic anomaly described here.

Magnetic anomaly due to a spherical object centered at (0, 0, z) is observed at point (x, y, 0) as

$$Ts\,(x, y, o) = P.\frac{(3\cos^2 I - 1)\cdot y^2 + (3\sin^2 I - 1)\cdot Z^2 - X^2 - 3\sin^2 I \cdot y \cdot Z}{(x^2 + y^2 + Z^2)^{5/2}}$$

where, y–axis is taken to the direction to the magnetic north and z–axis is vertically downward and

$(P = \frac{4}{3}\cdot \pi R^3 \cdot \Delta K \cdot To)$: Magnetic moment of the sphere,

R : Radius of the sphere,

$\Delta K = K_1 - K_2$: Difference of susceptibility between The sphere and its surrounding media,

T_0 : Intersity of geomagnetic field,

I : Inclination of geomagnetic field.

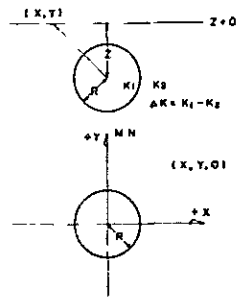

Magnetic anomaly due to dyke structure running to the direction at an angle of θ to the magnetic north is given in the following formula.

$$T_D(y, o) = \Delta K \cdot T_o (1 - \cos^2 I \cdot \sin^2 D) \cdot \sin d \left\{ \cos(2i - d - \frac{\pi}{2}) \cdot (\tan^{-1} \frac{y + \frac{w}{2}}{Z} - \tan^{-1} \frac{y - \frac{w}{2}}{Z}) + \sin(2i - d - \frac{\pi}{2}) \cdot \ln \frac{(y + \frac{w}{2})^2 + Z^2}{(y - \frac{w}{2})^2 + Z^2} \right\}$$

Here, y–axis is taken in the direction at an angle of $D(=90^o - \theta)$ to the magnetic north, i.e. the direction perpendicular to the trend of the dyke structure and z–axis is taken vertically downward to the upper surface of the dyke structure.

And

w	:	Width of the dyke structure,
$\Delta K = K_1 - K_2$	:	Difference of susceptibility between inside and outside the dyke,
To	:	Intensity of geomagnetic field,
I	:	Inclination of geomagnetic field,
d	:	Dip of the dyke,
$i = \tan^{-1}(\tan I / \cos D)$	:	Apparent inclination.

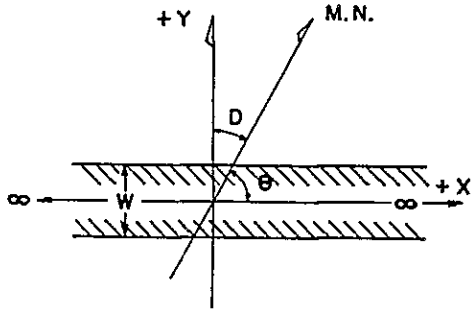

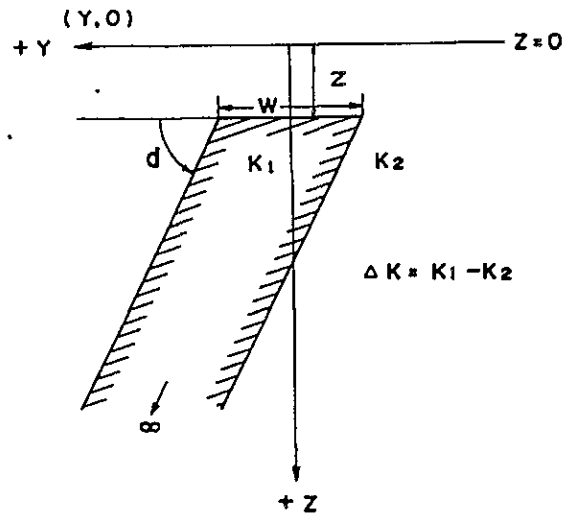

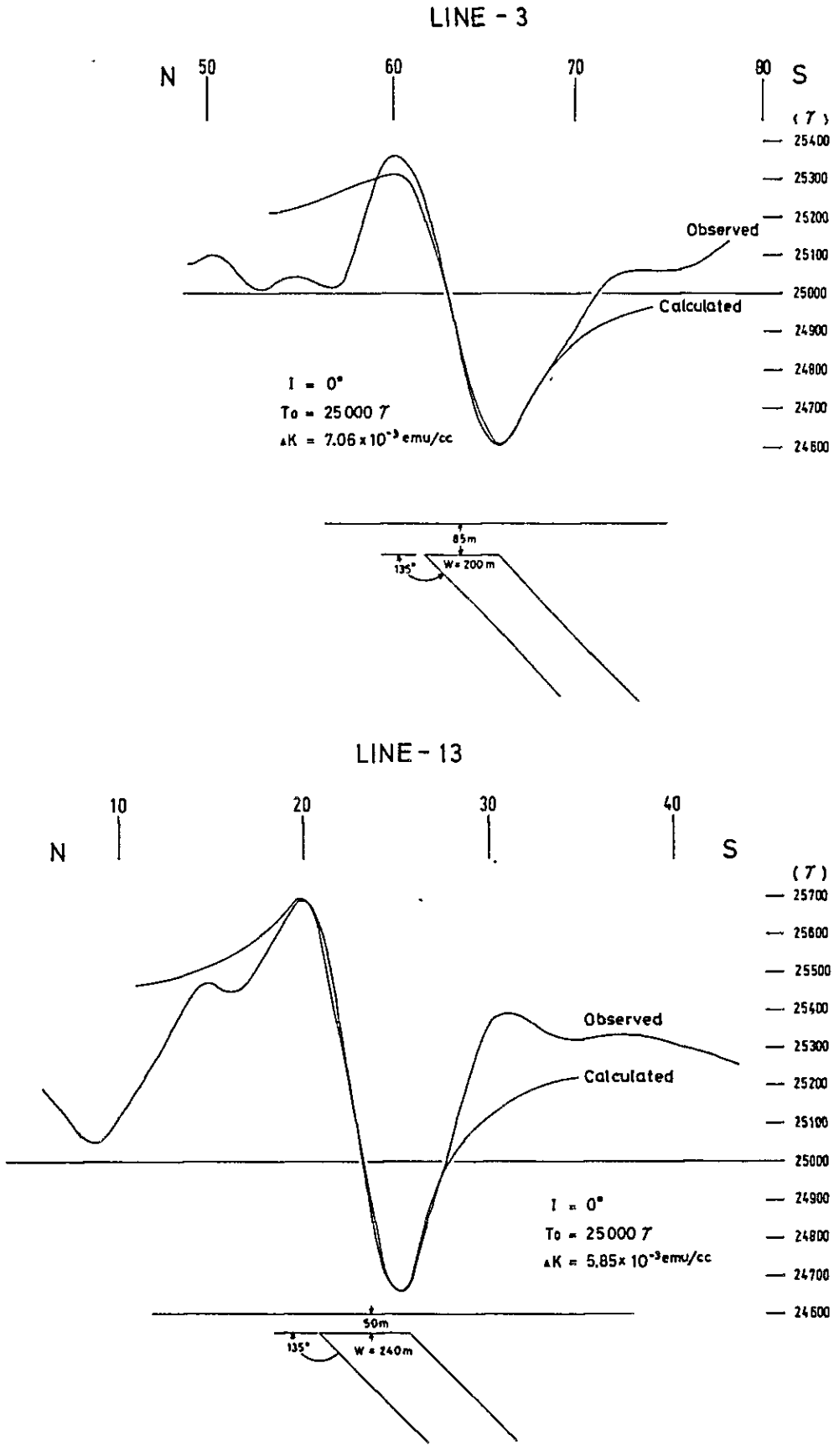

Fig. II–5–8 Magnetic Profiles

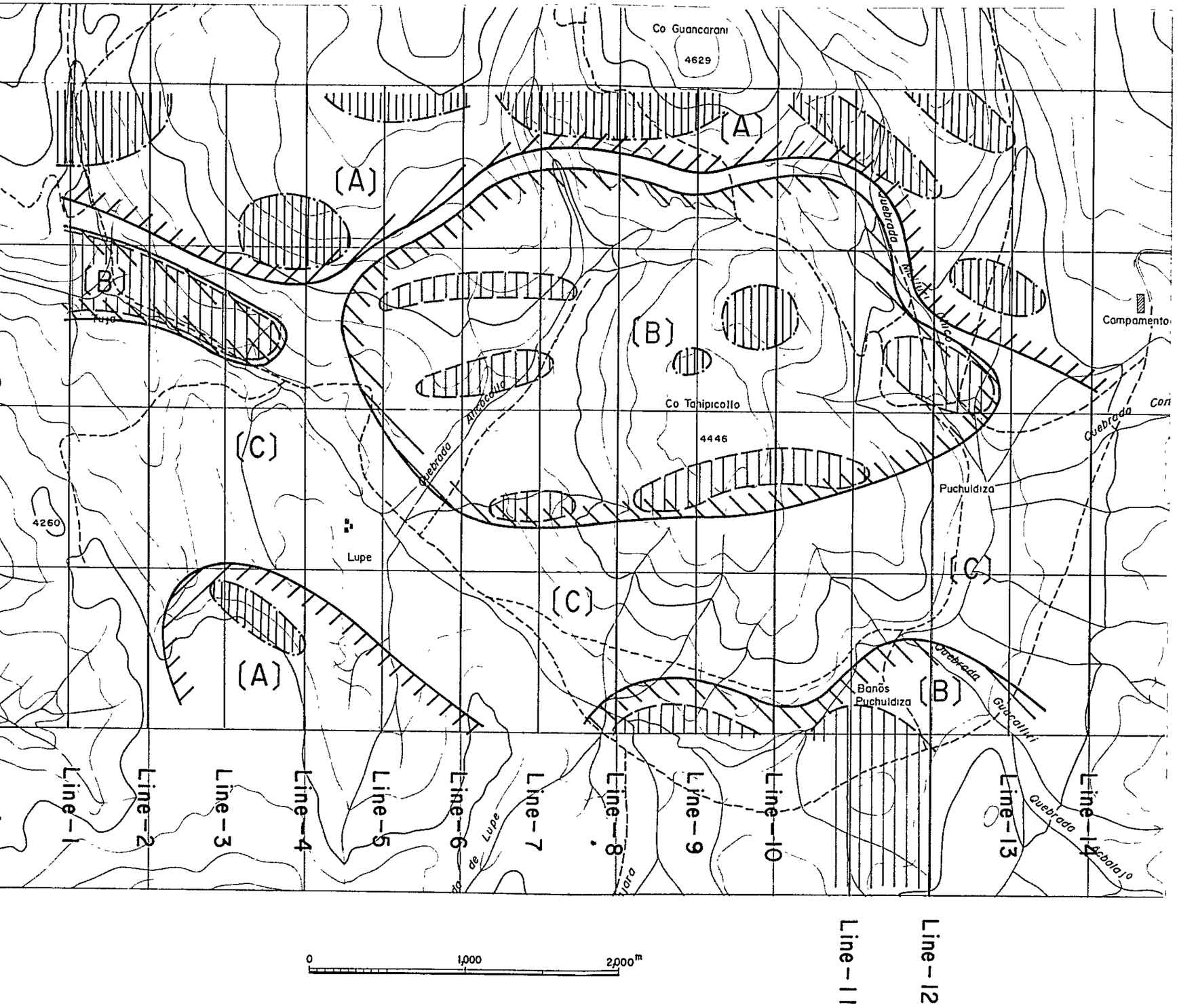

LEGEND

[A] Zone Where Highly Magnetized Bodies are Dominant.

[B] Zone Where Low Magnetic Susceptibility Rocks or Demagnetized Bodies are Dominant.

[C] Zone Where Rocks have Similar Magneti Susceptibility.

Highly Magnetized Body

Demagnetized Body

Fig II-5-9 ANALYTICAL MAP OF MAGNETIC SURVEY

PART III

SUMMARY

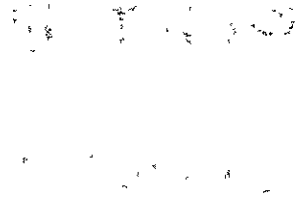

CHAPTER 1

SUMMARY OF THE SURVEY

Chapter 1 Summary of the Survey

The geothermal structures of the area were studied by various methods of geological, geochemical, electrical, magnetic and gravity surveys and the results are summarized as follows:

1–1 Geological Survey

With the purpose of clarifying the relationships between geologic structures and geothermal fluid, detailed geological survey was conducted in an area of 200km^2 covering the whole geothermal manifestations of the field.

The geothermal area is located on western range of Andes mountains and was the product of continuous faulting and block movements during the Andes orogenic period.

Churicollo formation, the lowest member encountered in the field shows complex geosynclinal structure and is covered by Tertiary and Quaternary formations such as rhyolitic white tuff, Puchuldiza andesitic rocks, and Lupe pyroclastic rocks. The formation shows gentle folding activity. Geological event indicates that Puchuldiza geothermal field has had twice main crustal disturbances that is, in early Tertiary age, and in Pliocene epoch.

Geologic structure in this area is characterized by tectonic lines of N–S, NW–SE trends, which are indicated by faults, block faulting, graben , and horst structures formed in the area. The graben structure, spreading through Tahipicollo and its western part was caused by above mentioned block faulting. This geologic activity as well as the presence of permeable layers is instrumental in forming the favorable condition for the reservoir of geothermal fluid.

1–2 Geochemical Survey

Geochemical survey is one of the tools used to find the nature of thermal fluid, to estimate the temperature of hot water in the aquifer, and to deduce the nature of fluid forming process. In the survey conducted at Puchuldiza geothermal fields, chemical analysis of hot water from exploratory wells and geysers, identification of clay minerals collected from altered zone by X–ray diffraction method, and Isotope examination of D/H and $^{18}0/^{16}0$ ratios were extensively used.

The result of the survey indicated that the springs rise to the surface through the fractured zone formed by different intersections of fault systems in the area.

Geochemistry confirmed that the hot water is weak alkali to neutral NaCl type. The temperature inferred from silica content and Na/K ratio of hot water suggests comparatively high temperature in the depth ranging from 190°C to 240°C.

Zonal arrangement of altered minerals shows that α–cristobalite prevailing in the surface and shallow part of the exploratory wells is not found in the depths of the wells and has been reverted to α–quartz. Clay minerals, such as chlorite, sericite and montmorillonite-sericite mixed

layers, which are produced under high temperature condition were detected in the core samples taken from deeper parts of the wells. Zeolite minerals, however, have not been observed except mordenite in the shallow parts of the well.

The result of Isotope study showed that hydrothermal water in the depth is a product of interaction between surface water and sub-surface rocks.

1–3 Gravity Survey

Gravity survey was conducted in the area of about 15 km in a east-west direction and about 10 km in a north–south direction covering Puchudiza and Tuja geothermal manifestations.

This gravity survey has a high density stations of 517 gravity points.

Since the survey area is located in the high Andean range, Bouguer anomaly shows a strong negative value due to Isostatic theory, but the relatively Bouguer anomaly shows 34 mgal gravity difference ranging from –273mgal to –307mgal.

Large scale gravity low–basin structure–was confirmed in the middle of survey area between Mt. Tahipicollo and Tuja. Around this basin a few faults of N–S and NW–SE predominate and these faults may possibly be the heat supply channels.

Moreover in this basin structure, thick sedimentation of permeable Tertiary white tuff (density of 2.0 – 2.4) under the andesitic flow as the cap rock is assumed. This structure serves, therefore, a good geothermal reservoir.

The circular arc of low gravity anomaly distribution seen in the first order residual map is of interest for future study. Additional gravity survey should be conducted around this area in order to know the extension of low gravity anomaly towards northwest.

1–4 Electrical Survey

In the determination of the resistivity structure in the area between Mt. Tahipicollo and Tuja, Schlumberger array using direct current resistivity method was made on two lines of 6 km each.

Resistivity anomalies in this area was divided into three groups. That is, upper high resistivity group corresponding to the compact andesitic lava, middle low resistivity group corresponding to the porous acidic tuff, and lower resistivity group corresponding to the basement tuffaceous rocks.

Porosity of acidic tuff is 15 – 25% and shows very low resistivity of 3 – 6 Ω m. Consequently, the layer seems to contain much hot saline water. Especially, in the eastern to northern part of Mt. Tahipicollo where five exploratory wells were drilled, extremely low resistivity value of 2.5–3.0 Ωm were detected, but the thickness of the reservoir is comparatively thin and the resistivity tends to increase with the depths.

In the western end of these lines, low resistivity anomalies of north–south trend were detected. Around Point 70 – 80 in the east of Tuja, high resistivity cap rock of andesite was

confirmed, and below this andesite, high temperature geothermal fluid is expected to be in low resistivity anomaly zone encountered.

Furthermore, in order to confirm the distribution of low resistivity anomaly in the depths, additional electrical survey should be carried out using the same method. Additional survey line of north–south trend along 501E and 502E are recommended to follow the distribution of above-mentioned low resistivity zone.

1–5 Magnetic Survey

Magnetic survey by means of proton magnetometer was adopted along 14 survey lines crossing Puchuldiza and Tuja geothermal manifestations with Tahipicollo as center.

In this area being close to the magnetic equator, the inclination is almost zero. Negative magnetic anomaly therefore should be detected above high magnetic source and contrarily positive anomaly over the low magnetic source or in demagnetized rocks because of the effect of geothermal fluids.

As the result of this survey indicated remarkable low magnetic anomaly is seen in the northern and southwestern area because of high susceptibility (10^{-3} emu/cc) of andesite present therein.

On the other hand, magnetic change is rarely seen in Tahipicollo, the center of the survey area. Comparatively high magnetic anomaly are widely distributed.

The existence of heat source in the depths is suggested because of wide decrease of susceptibility casued by demagnetization of geothermal alteration.

Around Puchuldiza and Tuja geothermal manifestations weak but high magnetic anomalies were detected suggesting weak demagnetization effect.

The interesting zone interpreted on the basis of the magnetic method is the area between east of Tuja and west of Ancocollo creek where the low magnetic bodies were confirmed in E–W direction. On the other hand,high magnetic belt extending NW to SE from exploratory well No. 3 and No. 4 seems to indicate the alteration of geothermal fluid as similarly shown by Puchuldiza anomalies.

CHAPTER 2

CONSIDERATION OF GEOTHERMAL SYSTEM

Chapter 2 Consideration of Geothermal System

2-1 Geologic Structure and Geothermal Fluid

The objective of geothermal exploration is to clarify the relationships between geologic structure having the favorable aquifer condition and the source of geothermal heat.

Most of the geothermal resources in the world exist in the graben zone with favorable conditions for the water reservoir that could transfer geothermal heat. If a volcano is somewhere around the graben structure, the place could be considered a promising area for geothermal development.

In general, the aquifer basin structure is controlled by the distribution of the permeable layers and the non-permeable layers, but as the high temperature water has very low viscosity coefficient, it is believed that the perfect non-permeable beds do not exist, unless the beds are solid without fractures. The structure to control the geothermal reservoir, therefore, is not the characteristics of the individual geological formation itself, but rather the combination of large geological structures.

In general, the effects of drainage of the geothermal effluent from the production well is considered to affect several kilometers. The subsurface water stream flow is not controlled by the porosity in a narrow sense, but controlled by the porosity in a broad sense, including the fine fractures.

Especially when considering the flow of low viscosity coefficient of the high temperature boiling water, even small cracks can not be disregarded.

Many surface geothermal manifestations do not necessary mean that favorable high temperature fluid reservoir exist at depth. Furthermore, the surface manifestations of the deep geothermal fluid may not necessarily be connected directly to the center of the high temperature geothermal reservoir.

In examining and analyzing the results of the survey, therefore, it is necessary to keep the above mentioned facts in mind in the interpretation of the survey results.

2-1-1 Survey result and geothermal activity

1) Geological structure in the area is characterized by the severe faulting and block movements during Andes orogeny.

   Geothermal manifestations distributed on the surface at Puchuliza and Tuja have occured at the intersection of different faults of N–S, NW–SE, and NE–SW trend systems.

   Hot water is rising to the surface along the fractured zone.

2) The scale and location of geothermal activity is controlled by the tectonic movement that continued from Cretaceous to Pliocene. This fact has been proved by the result of gravity survey. Presuming that over–280mgal is a high gravity area and

−290 mgal is a low gravity anomaly in the 20km^2 area surrounding Mt. Tahipicollo, the location of the center of geothermal field shows large scale depressed zone.
On the other hand, high gravity areas in the north, west, and southward surrounding depressed zone have shown upliftment of basement rocks. It shows that the geological structures in the Puchuldiza geothermal field have same gravity anomaly as most of the geothermal fields in the world with large scale graben structure.

3) Geological formation in this area consists of three groups, namely, Cretaceous basement rocks, Neogene Tertiary pyroclastics and Quaternary lava flow. Considering the physical properties of rocks such as the porosity and resistivity of rock samples from each formation, however, the geological formations can be classified into two groups as lower acidic pyroclastic formation and upper andesitic lava flows.
In general, resistivity of the geologic formation is mainly affected by the kind of rocks, porosity, components, and temperature of stream water, and it is commonly known that the area showing low resistivity anomaly less than 10 Ω m indicates the possible strata of geothermal reservoir.
The result of electrical prospecting measuring the resistivity of the formation, showed three layers, namely, upper high resistivity layer (100 – 3,000 Ω m), middle low resistivity layer (2 – 6 Ω m) and lower high resistivity layer (over 15 Ω m).
Where the upper high resistivity layer corresponds andesitic lava flow and low resistivity layer corresponds to layered acidic pyroclastics formation which underlie andesite lava flow. Judging from the result of resistivity survey the geothermal reservoir in this field is associated with acidic pyroclastic formation. In the magnetic survey, existence of thermally altered rocks in the underground shows high magnetic anomaly because of the demagnetization effect. Although small scale high magnetic anomalies were observed near Puchudiza and Tuja manifestations, the same high anomalies have appeared in wide areas from Mt. Tahipicollo to its western part.
Among the anomalies observed by the various geophysical method as shown in Fig. III−2−1 the distribution of gravity, electrical and magnetic anomalies have close relationship with geothermal reservoir and the tectonic lines crossing the anomalous zone. Judging from the map, the eastern part of Tuja manifestations is the western margin of low Bouguer anomaly. The low Bouguer anomaly can be considered as a promising zone for the future exploration.

4) The various physical properties of 47 rock samples taken at the site are shown in Table III−2−1. Interpretations of physical properties have been stated in Part II.

5) Based on the chemical analysis of hot water samples taken from several geysers and exploratory wells, the nature of hot water is neutral and NaCl type, with no noticeable differnce in chemical components.

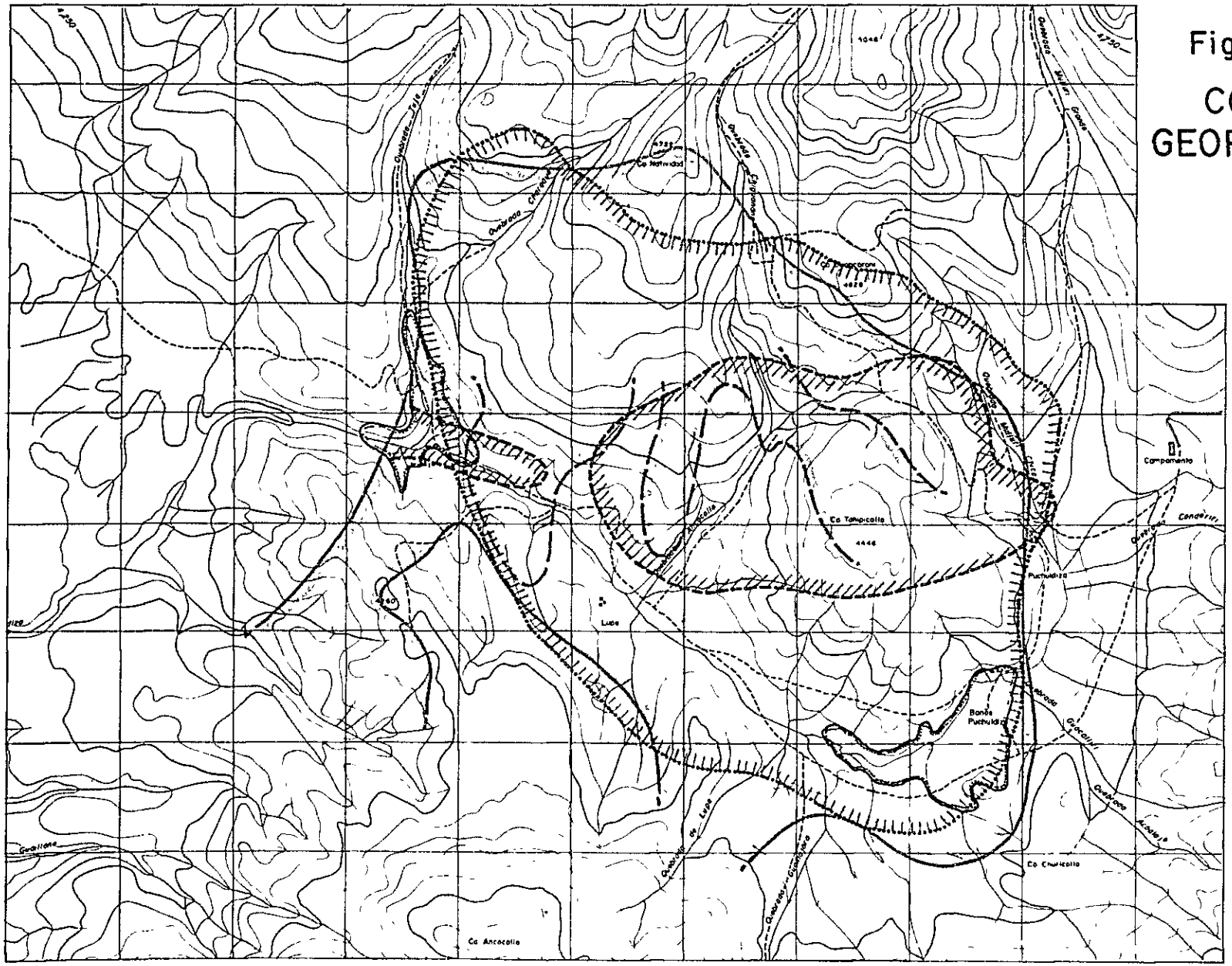

Fig Ⅲ-2-1

CONSOLIDATED GEOPHYSICAL ANOMALY

LEGEND

- Low Gravity anomaly
- Low Resistivity anomaly
- Low Magnetic anomaly

Table III–2–1 Physical Properties

No.	Period	Form	Rock type	Density N	Density W	Density D	Porosity (%)	Resis. (Ω·m)	Magneti. (10^{-4}emu/cc)	Sample No.	Remarks
1	Quaternary		Andesite	2.50	2.47	2.47	6.26	1900	–	0202	
2			"	2.54	2.56	2.51	8.53	200	2621	1206	
3			Andesitic Welded Tf.	2.35	2.31	2.34	7.54	390	605	1402	
4			"	2.55	2.52	2.53	5.83	720	2832	1403	
5			Andesite	2.44	2.43	2.43	7.39	690	–	1609	
6			"	2.46	2.47	2.45	6.64	920	3744	3001	
7			"	2.54	2.52	2.51	7.81	–	–	G–260	Gravity
8			"	2.62	2.62	2.60	4.55	–	–	G–287	"
9			"	2.25	2.28	2.23	14.28	–	–	G–300	"
10			"	2.52	2.51	2.50	4.40	–	–	G–343	"
11			"	2.52	2.52	2.50	5.05	–	–	G–389	"
12	Tertiary	Lupe F.	Andesite	2.43	2.38	2.39	7.58	1400	2033	0101	
13			Sand Stone	1.94	1.90	1.83	34.00	15	910	1205	
14			Conglomerate	2.40	2.89	2.37	9.21	–	–	G–377	Gravity
15		Puchuldiza F.	Andesitic Welded Tf.	2.34	2.36	2.30	7.92	9200	798	0102	
16			Basaltic Andesite	2.60	2.58	2.59	2.14	8400	–	0201	
17			Andesitic Welded Tf.	2.33	2.35	2.31	5.48	650	–	0302	
18			Basaltic Andesite	2.56	2.52	2.55	3.95	2600	713	1401	
19			"	2.54	2.54	2.53	2.50	270	1363	1610	
20			"	2.60	2.60	2.57	5.15	–	2398	2901	
21			Andesitic Welded Tf.	2.59	2.59	2.55	5.58	–	–	G–183	Gravity
22			Basaltic Andesite	2.81	2.30	2.28	5.30	–	–	G–372	"
23			"	2.51	2.51	2.49	3.78	–	–	G–373	"
24			"	2.38	2.38	2.39	13.94	–	–	G–375	"
25		Condoriri F.	Dacitic Tf.	2.13	2.21	2.05	21.83	–	–	0504	
26			"	2.00	2.00	1.99	24.84	320	188	1608	
27			Basaltic Andesite	2.41	2.40	2.36	11.86	–	1451	3006	
28			Dacitic Tf.	2.28	2.35	2.24	15.45	60	60	P–3(234)	Pozo-8 234m
29			"	2.30	2.36	2.26	15.44	85	58	P–4(310)	Pozo-4 310m
30		Choquechaya F.	Andesite (intrusion)	2.51	2.53	2.44	13.63	190	2374	1701	
31			Dacitic Tf.	2.43	2.46	2.36	15.78	66	76	P–5(540)	Pozo-5 540m
32		Utayane F.	Dacitic Welded Tf.	2.11	2.14	2.03	18.29	50	20	1613	
33			Conglomeratic SS	2.36	2.38	2.29	14.49	110	1827	1702	
34			Rhyolitic Tf.	2.17	2.24	2.12	16.50	130	16	1705	
35			Dacitic Welded Tf.	2.29	2.35	2.25	12.17	470	104	2801	
36			"	2.38	2.41	2.34	9.75	100	39	2802	
37			"	2.12	2.18	2.04	18.30	43	25	2803	
38			"	–	–	–	–	170	–	3002	
39			"	2.22	2.28	2.16	17.69	64	64	P–1(641)	Pozo-1 641m
40			"	2.40	2.43	2.36	11.26	170	115	P–1(697)	Pozo-1 697m
41			"	2.26	2.35	2.21	24.37	56	51	P–2(408)	Pozo-2 408m
42			"	2.39	2.43	2.34	13.21		60	P–2(522)	Pozo-2 522m
43			"	2.43	2.50	2.46	6.22		84	P–4(945)	Pozo-4 945m
44			"	2.42	2.42	2.36	11.81	290	293	P–5(1012)	Pozo-5 1012m
45	Cretaceous	Churicollo F.	Rhyolitic Tf.	2.34	2.39	2.30	12.21	380	78	1201	
46			"	2.35	2.39	2.32	11.68	120	83	1202	
47			"	2.36	2.40	2.30	12.18	110	58	1203	
48			Dacitic Welded Tf.	2.35	2.40	2.30	13.20	130	89	2201	
Total				47				33	32		

Therefore, the geothermal manifestations in the area are derived from the same heat source with same chemical homogeneous rocks in the sub-surface. Hot water selectively rise up to the surface along the fractured zone caused by fault.
The fractured zone is thinly covered by a cap rock of andesitic lava flows.

6) The reservoir temperature deduced from geothermometers applying silica content and Na/K ratios in hot water is comparatively high ranging from 190°C to 240°C.
Zonal arrangement of altered minerals examined by X–ray diffraction analysis has shown that α–cristobalite and montmorillonite prevailing in the shallow depth have been transformed into α–quartz, sericite, and montmorillonite – sericite mixed layer minerals. It means that temperature is increasing with depth.
According to the temperature logging of 5 wells, however, maximum temperatures are 130°C to 170°C. As sometimes observed the bottom temperature in some wells decreases with depth. Steam and water ratio in the flushing well is 1 to 6–10 with low enthalpy fluid.
The following should be considered:
   1. Location of exploratory wells drilled in the past might be far from the heat source.
   2. Convection of thermal fluid in aquifer is related with high permeability strata.
   3. Cold water from the shallow level mix with hot water in the depth.

   Based on the above, it will be necessary to investigate drilling cores, to do electrical logging of the wells, and to collect various informations for the future studies.

2–2 Hydrogeology of Geothermal System

1) The result of D/H and $^{18}O/^{16}O$ fractionation study has proven that geothermal fluid in this area is the product of cold meteoric water which permeate underground and thereby heated by the heat source existing in the depth and finally rise up to the surface along faults and fractures. Surface hot water activities are limited below 4,200m A. S. L. of the fault valley. Other geothermal manifestations above 4,200m A. S. L. have been observed as alteration zones.
As the water levels of 5 exploratory wells located around Mt. Tahipicollo is about 4,200m level, thermal water is overflowing spontaneously from the top of the well in case of well No. 1 which is located below 4,200m A. S. L.. Considering these facts, the water level around Mt. Tahipicollo is about 4,200m A. S. L. and the aquifer in the area is related with same geologic horizon.

2) According to the meteorological observation conducted by ENDESA, the annual rain fall in the area of 4,000m highland in the Tarapaca province, northern Chile is about 100mm. The annual volume of rainfall in the Puchuldiza geothermal field

is about 1 x 10^7 m^3 considering that the area is about 100km^2.
On the other hand, annual discharge from geysers at Puchuldiza and Tuja is calculated to be 1.7 x $10^6 m^3$, with the ratio of discharge and total rainfall as 0.17.
This ratio of 0.17 is the same value obtained in the measurement of the porosity of acidic pyroclastic formation considered as the aquifer of the geothermal fluid. Accordingly, 17% of total rainfall permeate underground and this shows that all discharge water from geothermal manifestations observed presently on the surface would be interpreted as meteoric water in origin. The result of isotopic study coincides also with above observations.

3) Water balance is maintained by natural flow, supposing however, that a 30MW geothermal power plant would be constructed in the field, recharge and water balance should be seriously considered. For example, if the steam and water ratio is 1:5, the discharge volume from the production wells for 30MW power generation is about 300 ton of steam and 1,500 ton of water per hour respectively. This means that circulation water derived from meteoric rain water is not sufficient because of 1.6 x $10^7 m^3$ required discharge volume per annum. As the aquifer of acidic pyroclastic layer is thick and spread widely in the area, water recharge for the aquifer from outside source should be reasonably considered.

4) In case the discharge volume of the geothermal fluid from the production wells is considerably more compared with water recharge of the aquifer, the water level in the underground would decrease at the nearby production wells and therefore, power output would also be unavoidably lowered. In order to maintain the pressure of the aquifer and to supply the geothermal fluid, it is advisable, therefore, to reinject the hot effluent back into the aquifer.
In certain geothermal plant in Japan, the effluent was initially discharged into the river after separation of steam. Consequently, the continuous draw off of hot water without replenishment gradually caused the drop of power output. To recover the loss power output, water injection was initiated and because of this remedial measure power output has gradually improved.

5) As the temperature of injection water is lower than the original hot water, it would naturally follow that the reinjected water will decrease the aquifer temperature. In some cases, therefore, water reinjection will be good for the maintenance of the high temperature of the aquifer because if cold water in the surface area would intrude instead of the reinjected water supplementing the discharged hot water, it will have more unfavorable effect on the aquifer. Considering the effect of reinjected water to the reservoir, it is necessary to study the location and depth of

the injection well carefully.

6) Kimura et al. (1965) pointed out that the flow of the underground water under natural conditions does not follow the Darcy flow as strictly assumed in the past but instead the flow was verified as Bingham flow. Accordingly, the natural flow of the water is not simply controlled by the porosity of the beds, but also flows along specific water channels. Even in the highly porous tuffaceous rocks, the hot spring water is flowing along fissures on the beds and along rock boundary and not flowing uniformly through tuffaceous rock.

   In case of high temperature geothermal fluid where the viscosity coefficient of the fluid is very low, even fine fissures of the formation should be considered as probable good pathway for the flow of geothermal fluid in the sub-surface layers.
   In water dominated geothermal field like Puchuldiza located in dry climate area, water equilibrium in the aquifer might pose serious problem in continuous operation of power plants. It is recommended therefore, that production well sites should be carefully sited in order to maintain stable geothermal power generation.

   In order to maintain water equilibrium, the recommended wells for further development were sited at places where the geothermal reservoir spread to deeper portion and where highly fractured zones are located for easy movement of supplementary fluid.

7) In the estimation of the behaviour of the geothermal fluid, however, many complicated parameters should be considered. Observation, therefore, of well water level, temperature and pressure change should be monitored continuously.

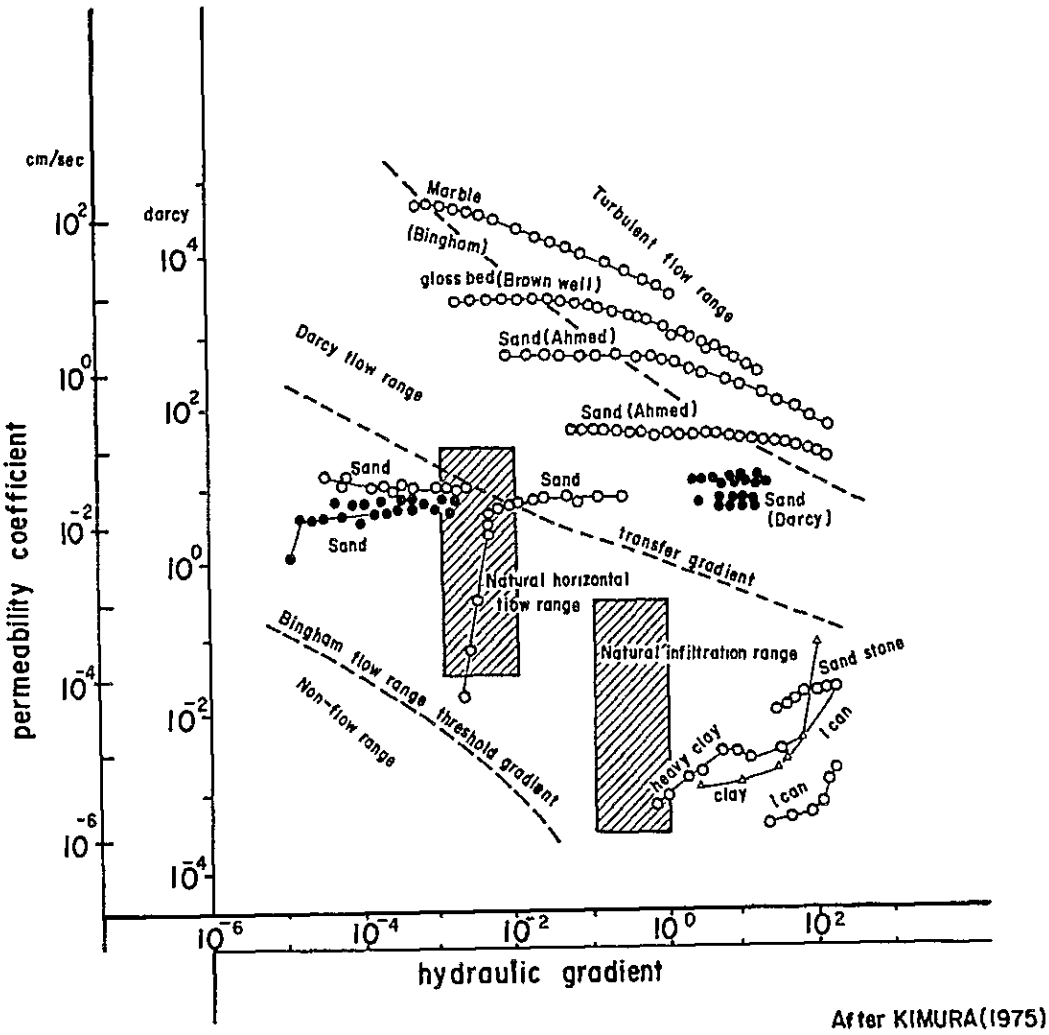

Fig.Ⅲ-2-2

FLOW OF NATURAL UNDERGROUND WATER

REFERENCES

References

((Unpublished report of Comite Geotermico-CORFO))

Healy, J., 1968, Geological Reconnaissance of Hot Spring Localities in Tarapaca and Antofagasta Province.

Healy, J., 1969, Geological Reconnaissance of Hot Spring Localities in Tarapaca and Antofagasta Province. (Second Interim Report)

A. Lahsen, 1969, Exploracion Geotermica en la Provincias de Tarapaca de Puchuldiza.

P. Trujillo, 1970, Manifestaciones Termales de Puchuldiza.

A. Lahsen, 1970, Informe Preliminar Sobre la Geologia de Puchuldiza.

A. Lahsen, 1973, Geologia de Puchuldiza.

A. Lahsen, 1975, Evaluacion del Sistema Geotermico de Puchuldiza.

P. Trujillo, 1977, The Puchuldiza Geothermal Field.

A. Lahsen, 1978, Evaluacion de los Resultados de la Exploracion del Campo Geotermico de Puchuldiza, Region Tarapaca.

((Published Report))

Cristi, J., Hand Book of South American Geology p. 189–214.

Vicente, C., 1970, Liminary and Geosynclinal Andes Major Orogenic Phases and Synchronical Evolutions of the Central Andes, Buenos Aires Solid Earth Problem Conference, p. 451–470.

James, D., 1973, The Evolution of the Andes, Continents Adrift by J. Wilson.

A. Lahsen, and P. Trujillo, 1975, The geothermal Field of El Tatio, Chile. Second United Nations Symposium, p. 157–176.

Bhattachaya, P.K. and H.P. Patra, 1968, Direct Current Geoelectric Sounding, Method in Geochemistry and Geophysics 9, Elsevier.

Onodera, S., 1975, An Evaluation of Geothermal Potential by Resistivity Sounding Curves, Second United Nations Symposium, p. 1167–1174.

D. R. Mabey et al, 1978, Reconnaissance Geophysical Studies of the Geothermal System in Southern Raft River Valley, Idaho, Geophysics, v.43, no.7, p. 1470–1469.

Tripp, A.C. et al, 1978, Electromagnetic and Schulumberger resistivity Sounding in the Roosevelt Hot Spring KGRA, Geophysics, v. 43, no. 7, p. 1450–1469.

Ward, S.H. et al, 1978, A summary of the Geology, Geochemistry, and Geophysics of the Roosevelt Hot Springs Thermal Area, Utah, Geophysics, v. 43, no.7, p.1515–1542.

Onodera, S., 1971, Geophysical Exploration for Geothermal Field, Kyushu University.

Bott, M.H.P., 1959, The Use of Electronic Digital Computers for the Evaluation of Gravimetric Corrections, Geophysical Prospecting, v. 7, p. 45.

PHOTOGRAPHS

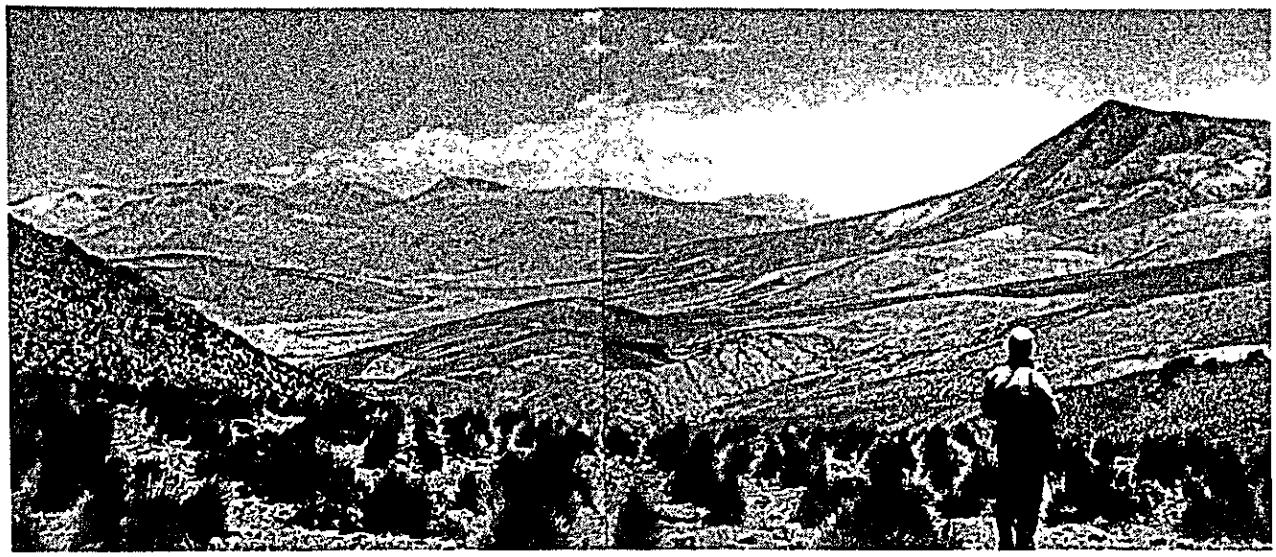

Survey Area (Right side : C_o.Condoriri 4,862m elevation)

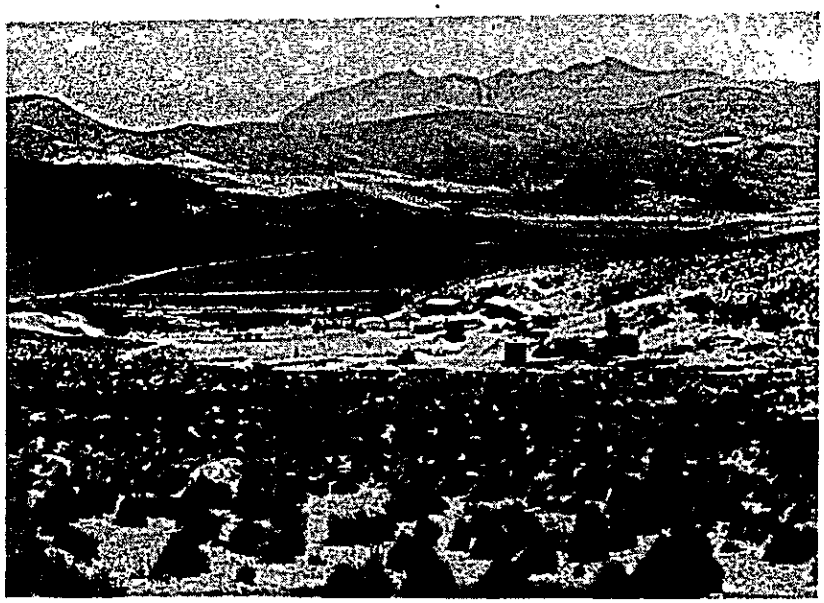

Camp site

Geothermal Well
(Pozo 3)

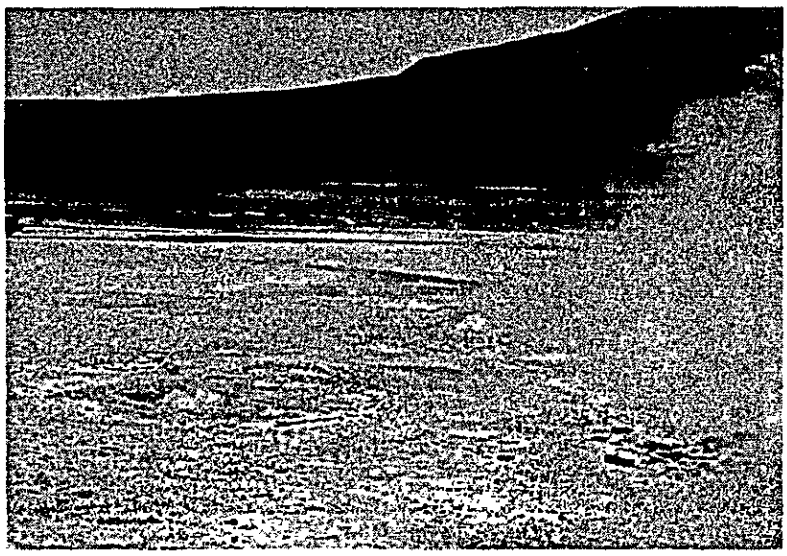

Puchuldiza Manifestation

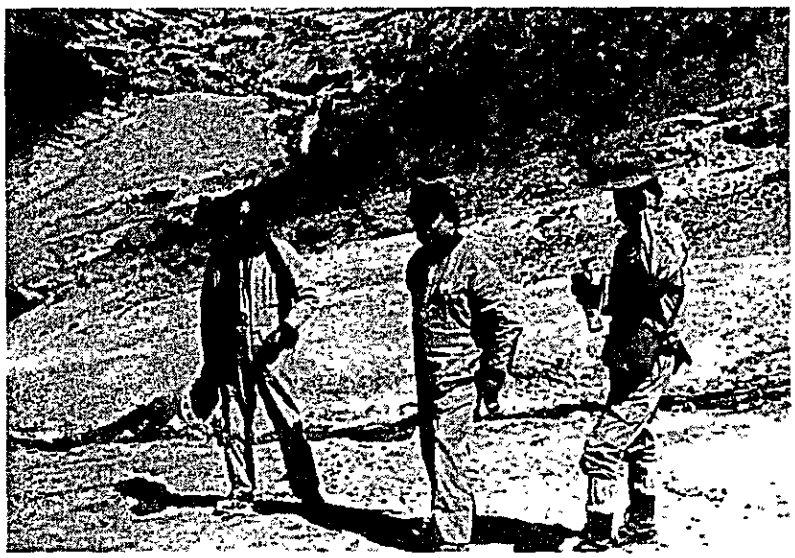

Geological Survey

Gravity Survey

Electrical Survey

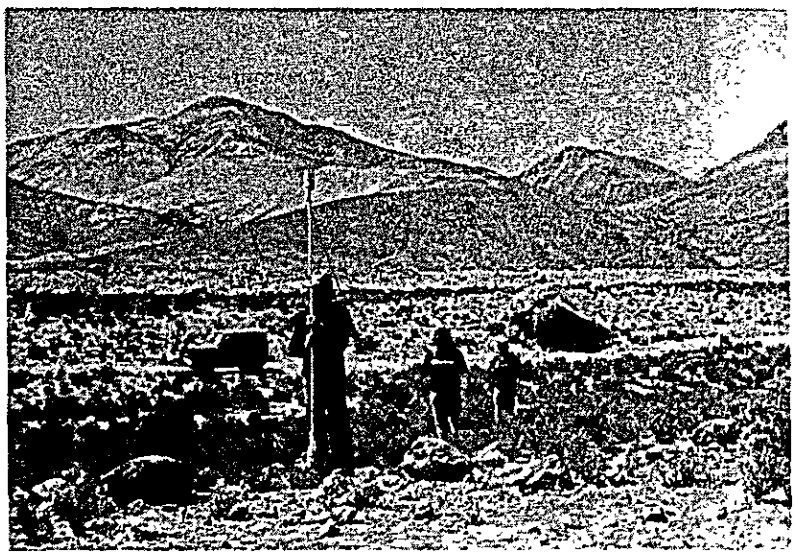

Magnetic Survey

VES CURVES

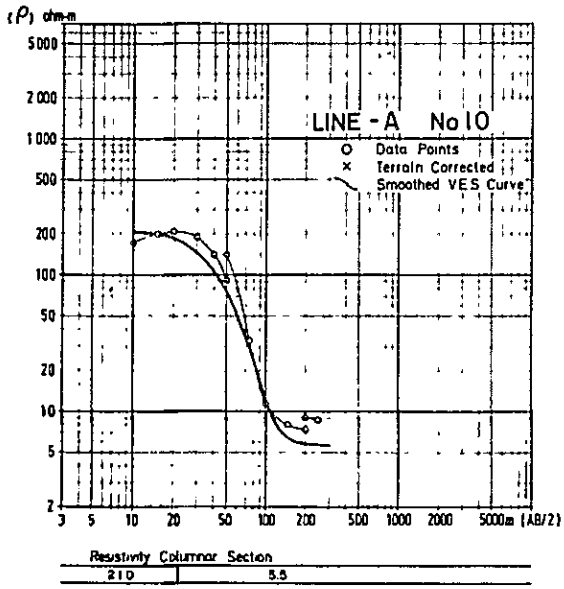
(ρ) ohm-m
LINE - A No 10
O Data Points
× Terrain Corrected
Smoothed VES Curve
5000
2000
1000
500
200
100
50
20
10
5
2
3 5 10 20 50 100 200 500 1000 2000 5000m (AB/2)
Resistivity Columnar Section
210
5.5

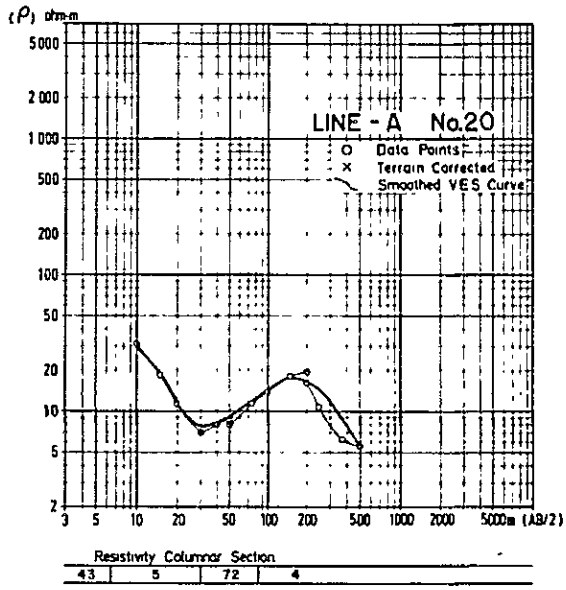
(ρ) ohm-m
LINE - A No.20
O Data Points
× Terrain Corrected
Smoothed VES Curve
5000
2000
1000
500
200
100
50
20
10
5
2
3 5 10 20 50 100 200 500 1000 2000 5000m (AB/2)
Resistivity Columnar Section
43
5
72
4

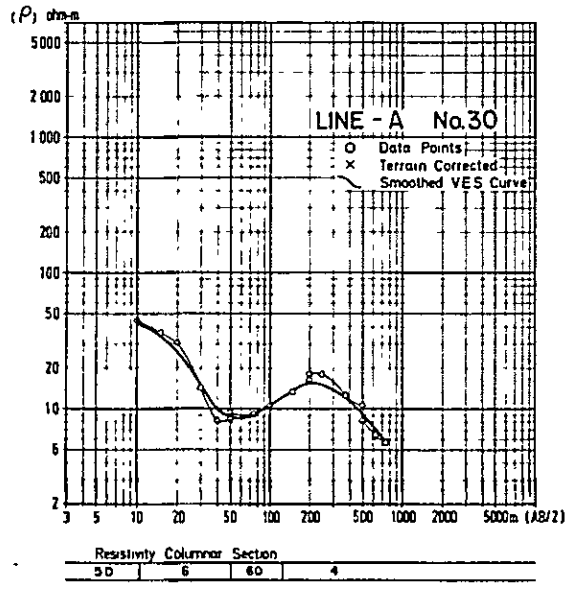
(ρ) ohm-m
LINE - A No.30
O Data Points
× Terrain Corrected
Smoothed VES Curve
5000
2000
1000
500
200
100
50
20
10
6
2
3 5 10 20 50 100 200 500 1000 2000 5000m (AB/2)
Resistivity Columnar Section
50
6
60
4

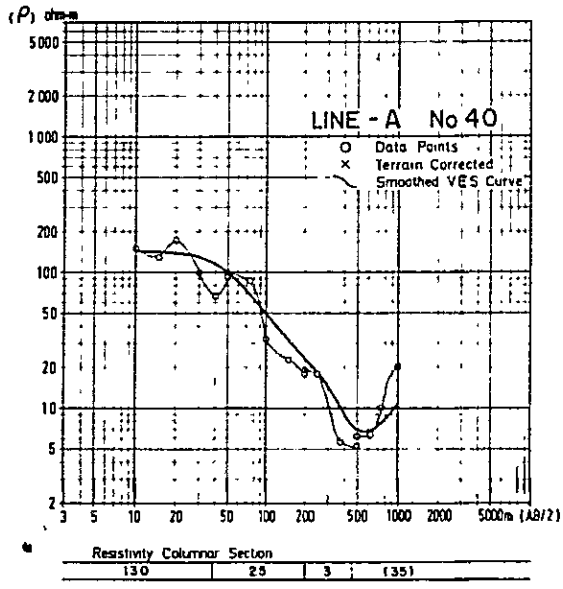
(ρ) ohm-m
LINE - A No 40
O Data Points
× Terrain Corrected
Smoothed VES Curve
5000
2000
1000
500
200
100
50
20
10
5
2
3 5 10 20 50 100 200 500 1000 2000 5000m (AB/2)
Resistivity Columnar Section
130
25
3
(35)

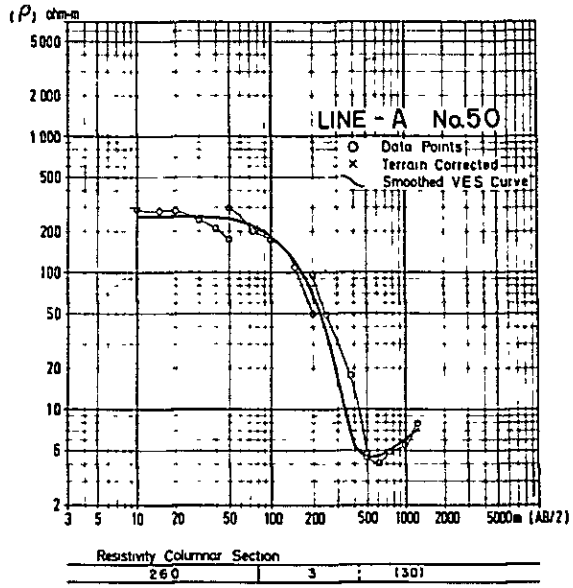
(ρ) ohm-m
LINE - A No.50
O Data Points
× Terrain Corrected
Smoothed VES Curve
5000m (AB/2)
Resistivity Columnar Section
260
3
(30)

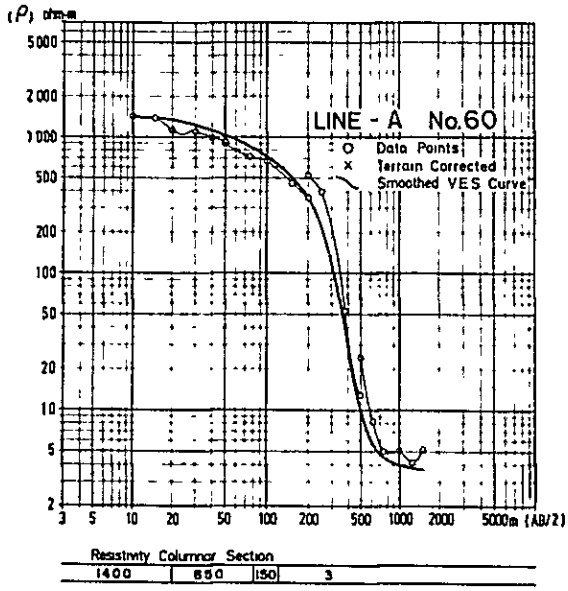
(ρ) ohm-m
LINE - A No.60
O Data Points
× Terrain Corrected
Smoothed VES Curve
5000m (AB/2)
Resistivity Columnar Section
1400
650
150
3

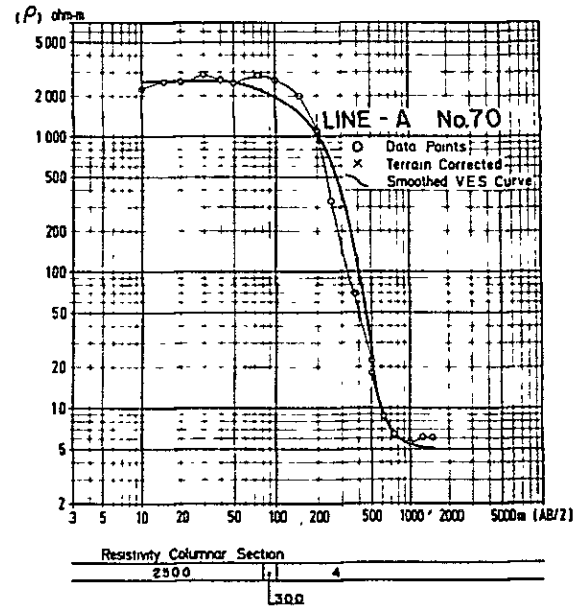
(ρ) ohm-m
LINE - A No.70
O Data Points
× Terrain Corrected
Smoothed VES Curve
5000m (AB/2)
Resistivity Columnar Section
2500
4
300

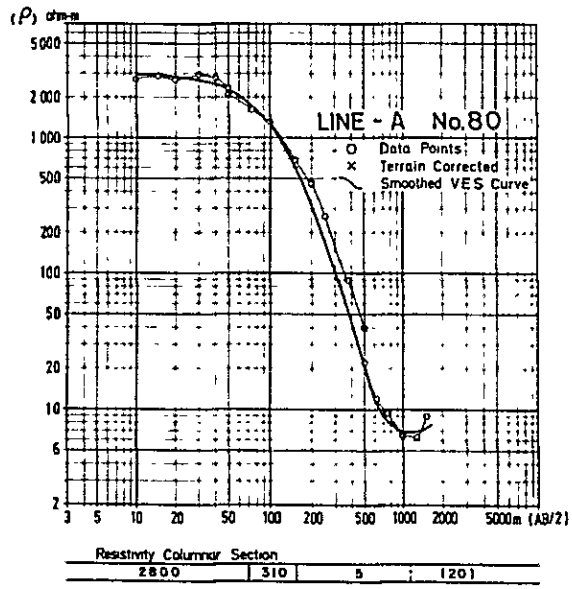
(ρ) ohm-m
LINE - A No.80
O Data Points
× Terrain Corrected
Smoothed VES Curve
5000m (AB/2)
Resistivity Columnar Section
2800
310
5
(20)

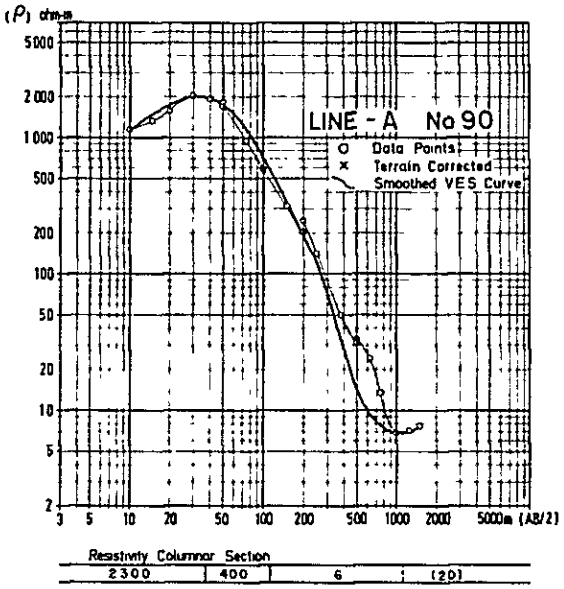
(ρ) ohm-m
LINE - A No 90
O Data Points
× Terrain Corrected
Smoothed VES Curve
5000
2000
1000
500
200
100
50
20
10
5
2
3 5 10 20 50 100 200 500 1000 2000 5000m (AB/2)
Resistivity Columnar Section
2300 400 6 (20)

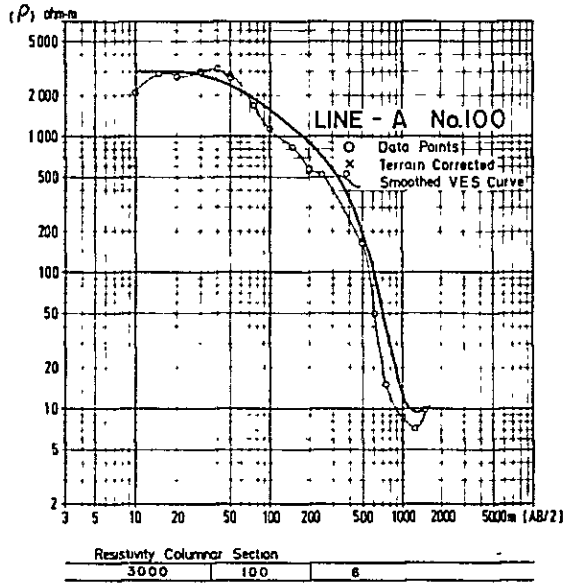
(ρ) ohm-m
LINE - A No.100
O Data Points
× Terrain Corrected
Smoothed VES Curve
5000
2000
1000
500
200
100
50
20
10
5
2
3 5 10 20 50 100 200 500 1000 2000 5000m (AB/2)
Resistivity Columnar Section
3000 100 6

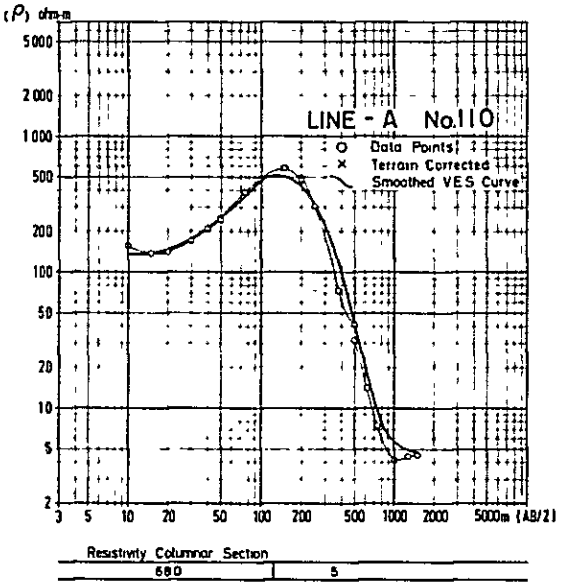
(ρ) ohm-m
LINE - A No.110
O Data Points
× Terrain Corrected
Smoothed VES Curve
5000
2000
1000
500
200
100
50
20
10
5
2
3 5 10 20 50 100 200 500 1000 2000 5000m (AB/2)
Resistivity Columnar Section
680 5

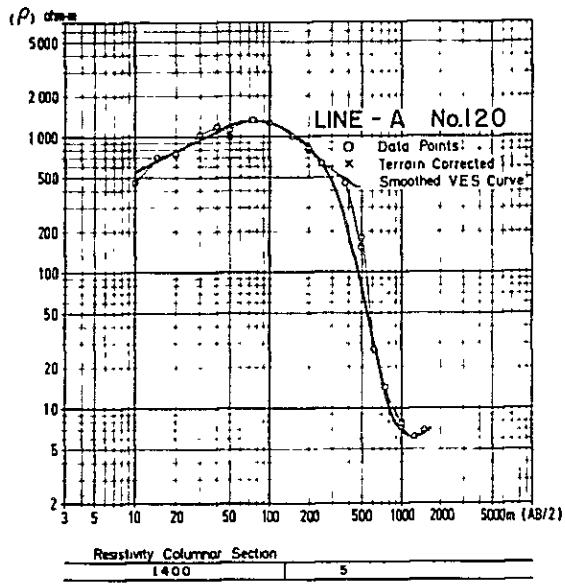
(ρ) ohm-m
LINE - A No.120
O Data Points
× Terrain Corrected
Smoothed VES Curve
5000
2000
1000
500
200
100
50
20
10
5
2
3 5 10 20 50 100 200 500 1000 2000 5000m (AB/2)
Resistivity Columnar Section
1400 5

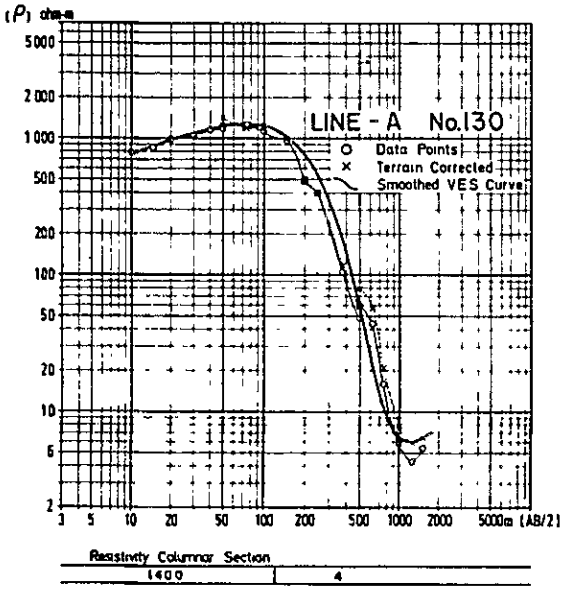
(ρ) ohm-m
LINE - A No.130
O Data Points
× Terrain Corrected
Smoothed VES Curve
AB/2
Resistivity Columnar Section
1400
4

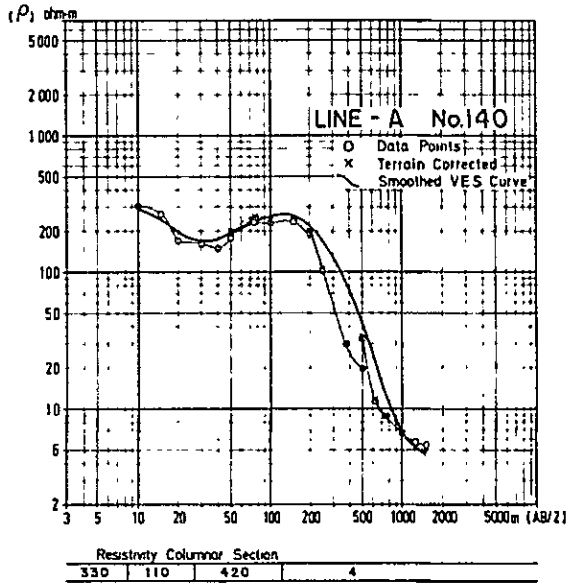
(ρ) ohm-m
LINE - A No.140
O Data Points
× Terrain Corrected
Smoothed VES Curve
AB/2
Resistivity Columnar Section
330
110
420
4

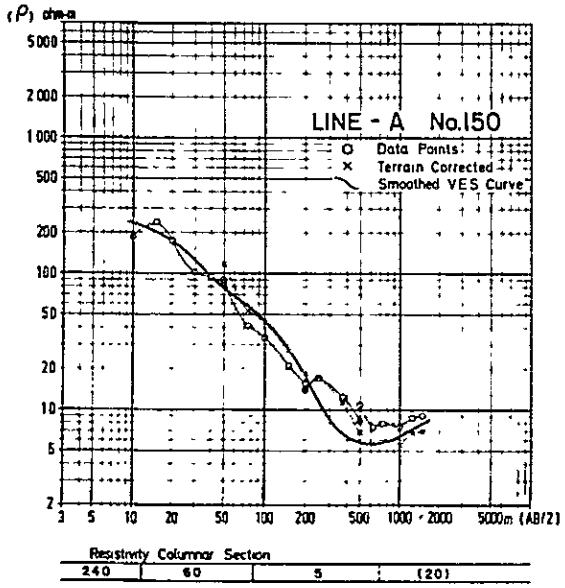
(ρ) ohm-m
LINE - A No.150
O Data Points
× Terrain Corrected
Smoothed VES Curve
AB/2
Resistivity Columnar Section
240
60
5
(20)

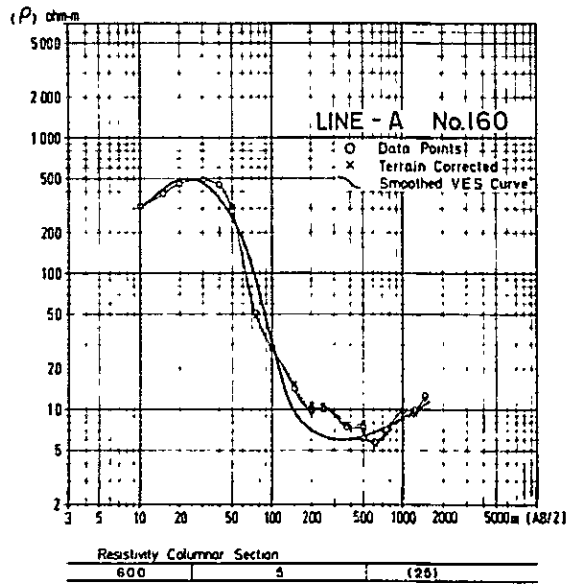
(ρ) ohm-m
LINE - A No.160
O Data Points
× Terrain Corrected
Smoothed VES Curve
AB/2
Resistivity Columnar Section
600
5
(25)

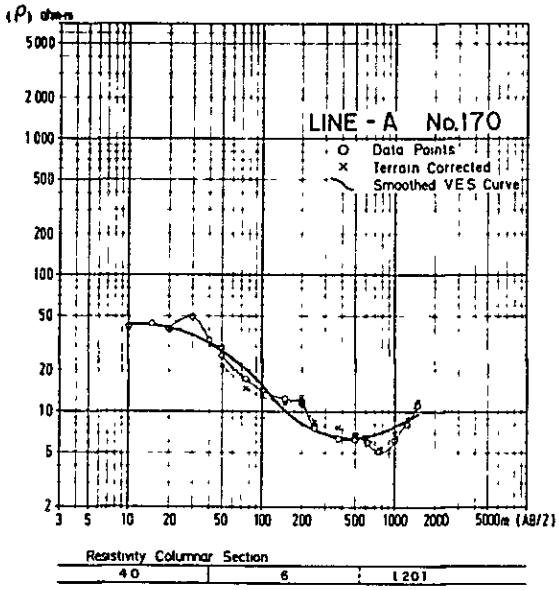
(ρ) ohm-m
LINE - A No.170
O Data Points
× Terrain Corrected
Smoothed VES Curve
5000
2000
1000
500
200
100
50
20
10
5
2
3 5 10 20 50 100 200 500 1000 2000 5000m (AB/2)
Resistivity Columnar Section
40 | 6 | (20)

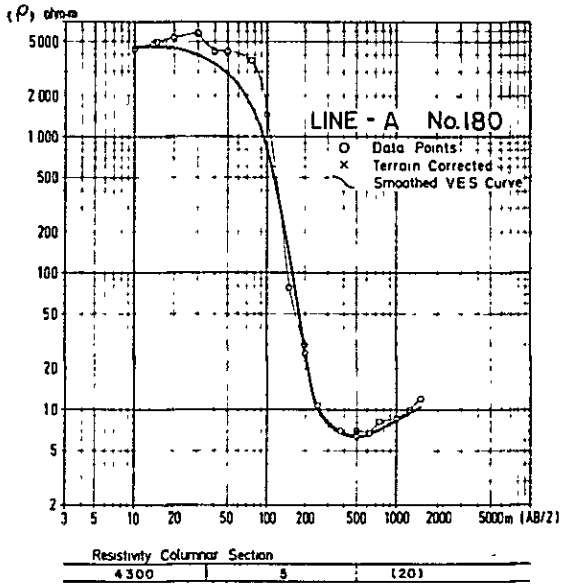
(ρ) ohm-m
LINE - A No.180
O Data Points
× Terrain Corrected
Smoothed VES Curve
5000
2000
1000
500
200
100
50
20
10
5
2
3 5 10 20 50 100 200 500 1000 2000 5000m (AB/2)
Resistivity Columnar Section
4300 | 5 | (20)

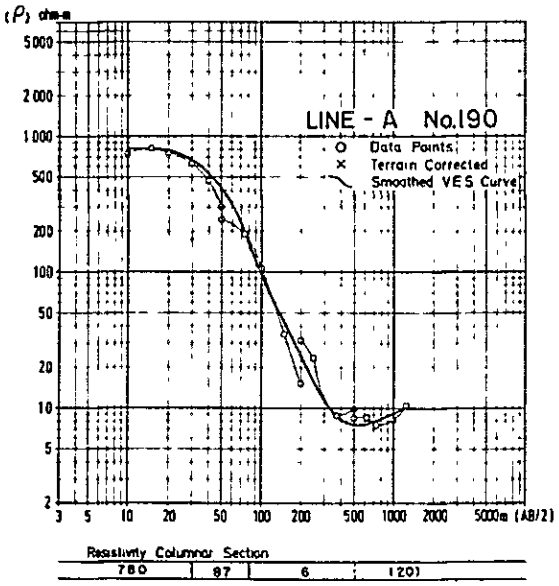
(ρ) ohm-m
LINE - A No.190
O Data Points
× Terrain Corrected
Smoothed VES Curve
5000
2000
1000
500
200
100
50
20
10
5
2
3 5 10 20 50 100 200 500 1000 2000 5000m (AB/2)
Resistivity Columnar Section
780 | 97 | 6 | (20)

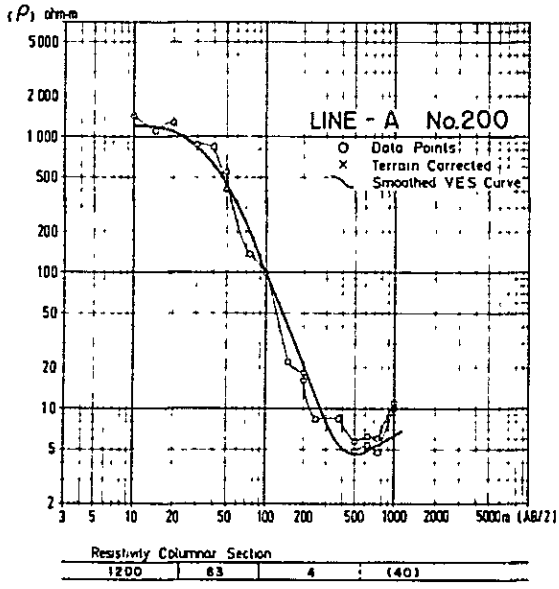
(ρ) ohm-m
LINE - A No.200
O Data Points
× Terrain Corrected
Smoothed VES Curve
5000
2000
1000
500
200
100
50
20
10
5
2
3 5 10 20 50 100 200 500 1000 2000 5000m (AB/2)
Resistivity Columnar Section
1200 | 83 | 4 | (40)

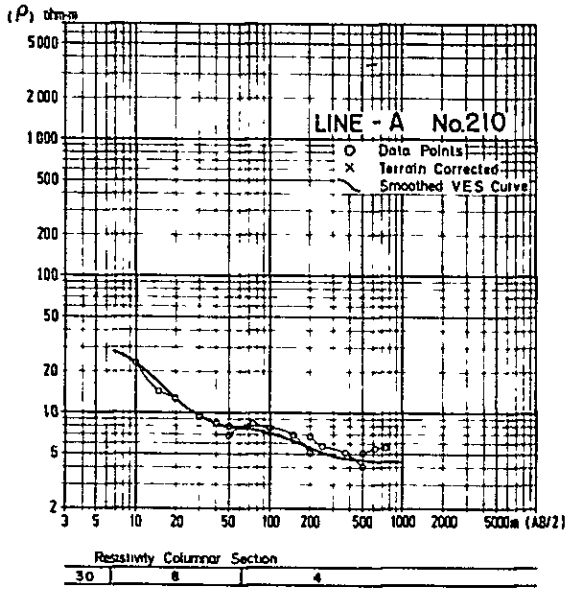
(ρ) ohm-m
5000
2000
1000
500
200
100
50
20
10
5
2
3 5 10 20 50 100 200 500 1000 2000 5000m (AB/2)
LINE - A No.210
O Data Points
× Terrain Corrected
Smoothed VES Curve
Resistivity Columnar Section
30
8
4

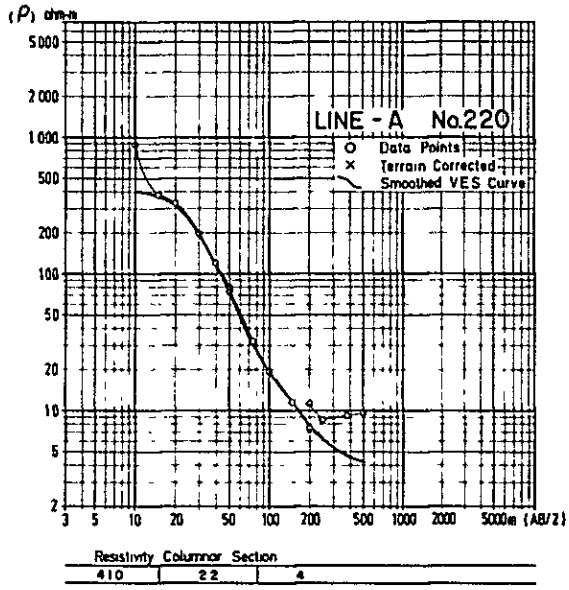
(ρ) ohm-m
5000
2000
1000
500
200
100
50
20
10
5
2
3 5 10 20 50 100 200 500 1000 2000 5000m (AB/2)
LINE - A No.220
O Data Points
× Terrain Corrected
Smoothed VES Curve
Resistivity Columnar Section
410
22
4

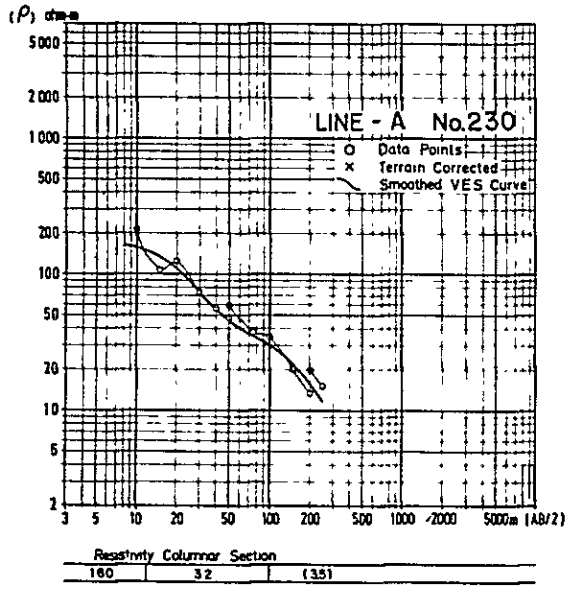
(ρ) ohm-m
5000
2000
1000
500
200
100
50
20
10
5
2
3 5 10 20 50 100 200 500 1000 2000 5000m (AB/2)
LINE - A No.230
O Data Points
× Terrain Corrected
Smoothed VES Curve
Resistivity Columnar Section
160
32
(35)

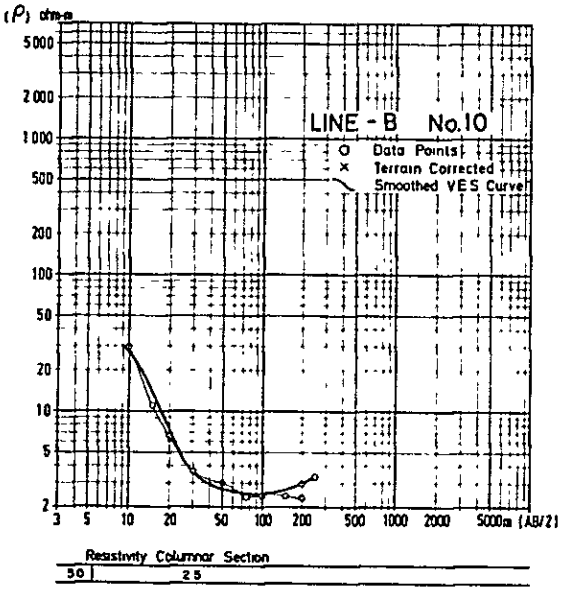
(ρ) ohm-m
LINE - B No.10
O Data Points
× Terrain Corrected
Smoothed VES Curve
5000
2000
1000
500
200
100
50
20
10
5
2
3 5 10 20 50 100 200 500 1000 2000 5000m (AB/2)
Resistivity Columnar Section
50
25

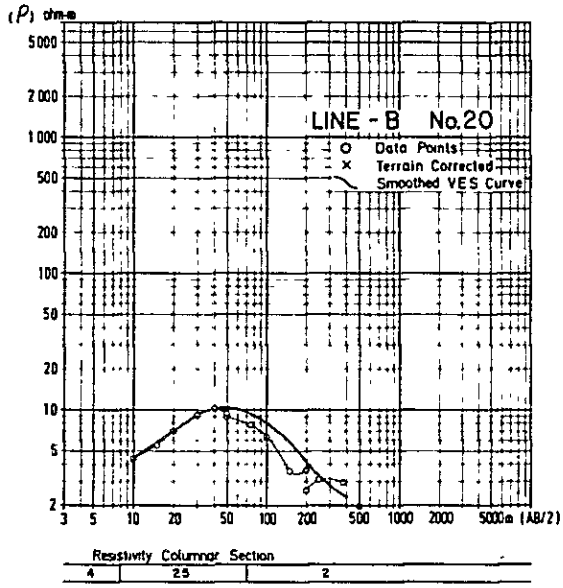
(ρ) ohm-m
LINE - B No.20
O Data Points
× Terrain Corrected
Smoothed VES Curve
5000
2000
1000
500
200
100
50
20
10
5
2
3 5 10 20 50 100 200 500 1000 2000 5000m (AB/2)
Resistivity Columnar Section
4
25
2

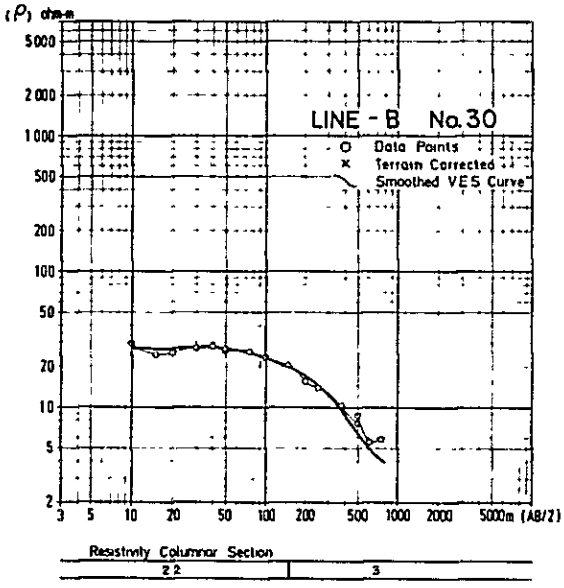
(ρ) ohm-m
LINE - B No.30
O Data Points
× Terrain Corrected
Smoothed VES Curve
5000
2000
1000
500
200
100
50
20
10
5
2
3 5 10 20 50 100 200 500 1000 2000 5000m (AB/2)
Resistivity Columnar Section
22
3

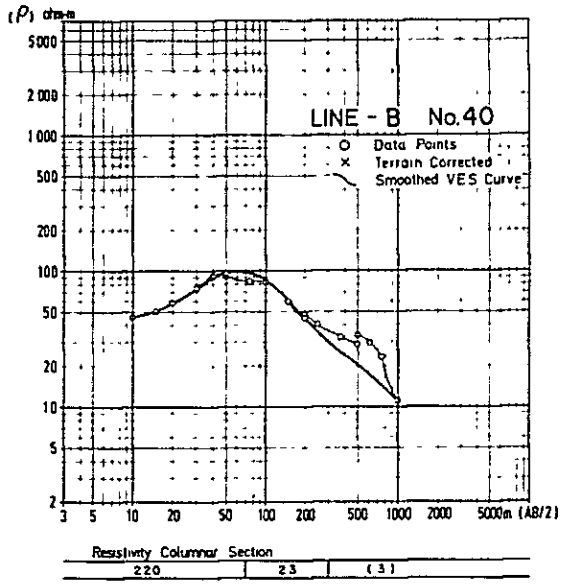
(ρ) ohm-m
LINE - B No.40
O Data Points
× Terrain Corrected
Smoothed VES Curve
5000
2000
1000
500
200
100
50
20
10
5
2
3 5 10 20 50 100 200 500 1000 2000 5000m (AB/2)
Resistivity Columnar Section
220
23
(3)

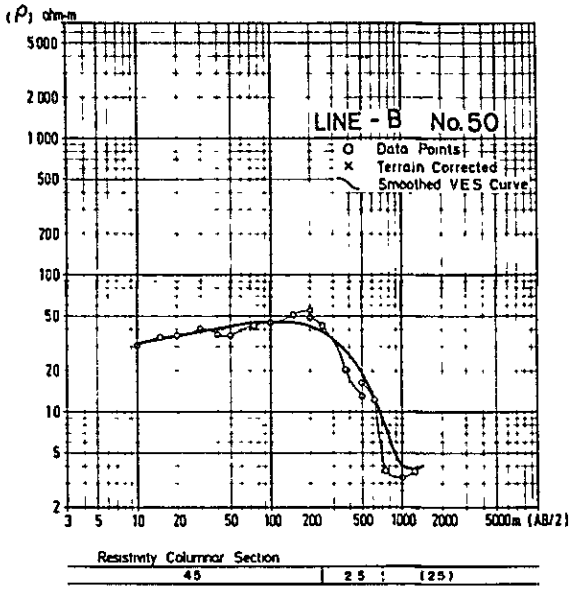
(ρ) ohm-m
LINE - B No.50
O Data Points
× Terrain Corrected
Smoothed VES Curve
5000
2000
1000
500
200
100
50
20
10
5
2
3 5 10 20 50 100 200 500 1000 2000 5000m (AB/2)
Resistivity Columnar Section
45
25
(25)

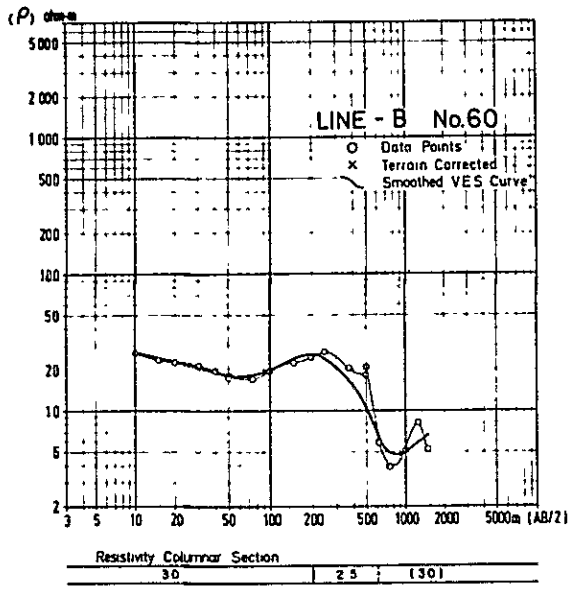
(ρ) ohm-m
LINE - B No.60
O Data Points
× Terrain Corrected
Smoothed VES Curve
5000
2000
1000
500
200
100
50
20
10
5
2
3 5 10 20 50 100 200 500 1000 2000 5000m (AB/2)
Resistivity Columnar Section
30
25
(30)

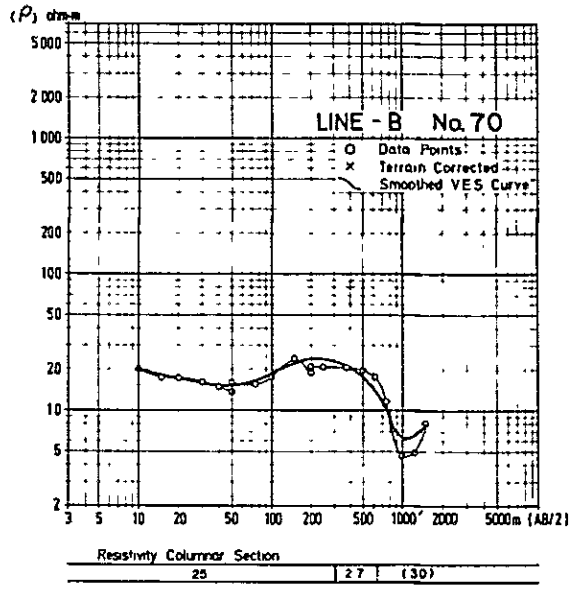
(ρ) ohm-m
LINE - B No.70
O Data Points
× Terrain Corrected
Smoothed VES Curve
5000
2000
1000
500
200
100
50
20
10
5
2
3 5 10 20 50 100 200 500 1000 2000 5000m (AB/2)
Resistivity Columnar Section
25
27
(30)

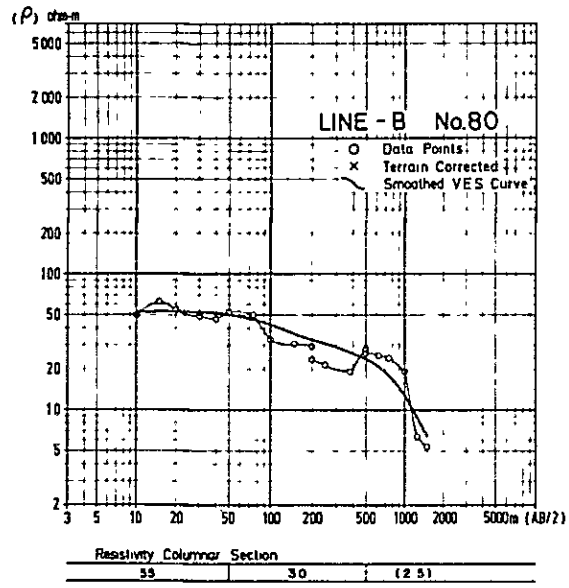
(ρ) ohm-m
LINE - B No.80
O Data Points
× Terrain Corrected
Smoothed VES Curve
5000
2000
1000
500
200
100
50
20
10
5
2
3 5 10 20 50 100 200 500 1000 2000 5000m (AB/2)
Resistivity Columnar Section
55
30
(25)

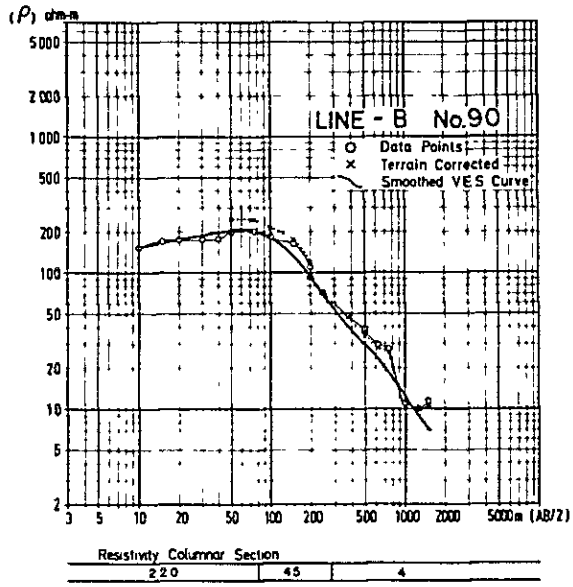
(ρ) ohm-m
LINE - B No.90
O Data Points
× Terrain Corrected
Smoothed VES Curve
5000
2000
1000
500
200
100
50
20
10
5
2
3 5 10 20 50 100 200 500 1000 2000 5000m (AB/2)
Resistivity Columnar Section
220 45 4

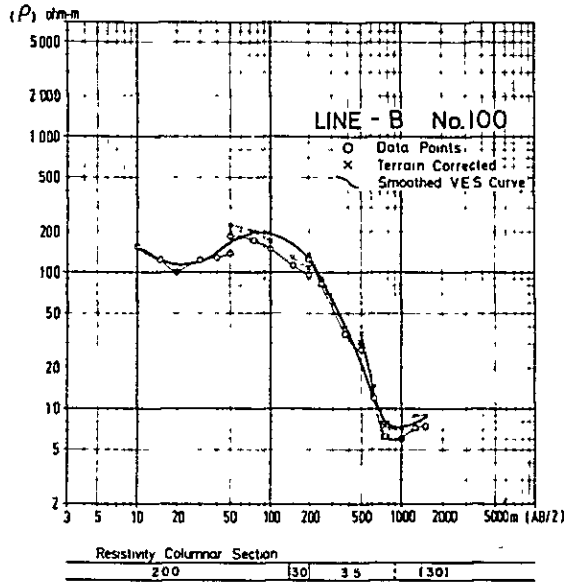
(ρ) ohm-m
LINE - B No.100
O Data Points
× Terrain Corrected
Smoothed VES Curve
5000
2000
1000
500
200
100
50
20
10
5
2
3 5 10 20 50 100 200 500 1000 2000 5000m (AB/2)
Resistivity Columnar Section
200 30 35 (30)

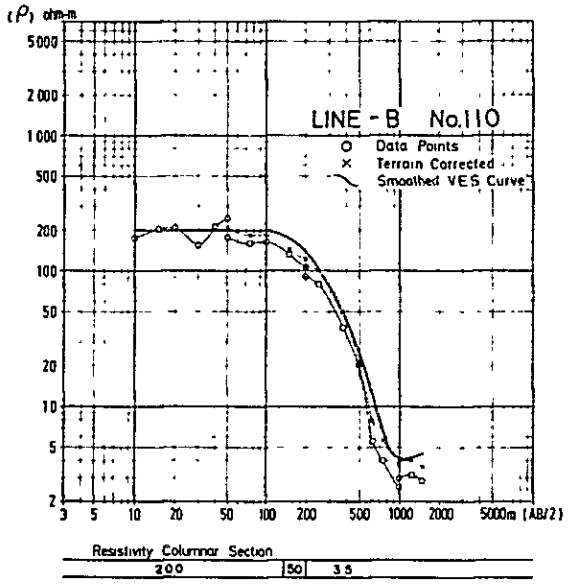
(ρ) ohm-m
LINE - B No.110
O Data Points
× Terrain Corrected
Smoothed VES Curve
5000
2000
1000
500
200
100
50
20
10
5
2
3 5 10 20 50 100 200 500 1000 2000 5000m (AB/2)
Resistivity Columnar Section
200 50 35

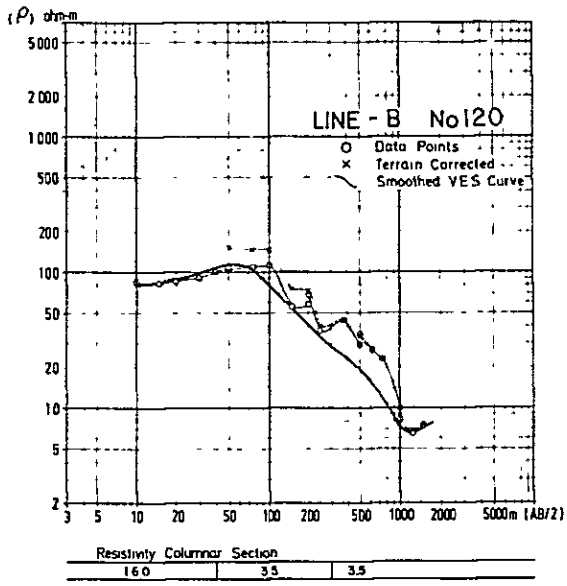
(ρ) ohm-m
LINE - B No120
O Data Points
× Terrain Corrected
Smoothed VES Curve
5000
2000
1000
500
200
100
50
20
10
5
2
3 5 10 20 50 100 200 500 1000 2000 5000m (AB/2)
Resistivity Columnar Section
160 35 35

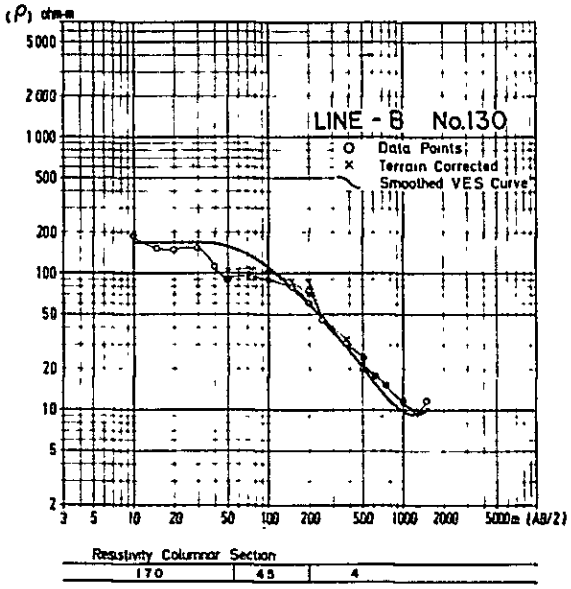
(ρ) ohm-m
LINE - B No.130
O Data Points
× Terrain Corrected
Smoothed VES Curve
5000
2000
1000
500
200
100
50
20
10
5
2
3 5 10 20 50 100 200 500 1000 2000 5000m (AB/2)
Resistivity Columnar Section
170
45
4

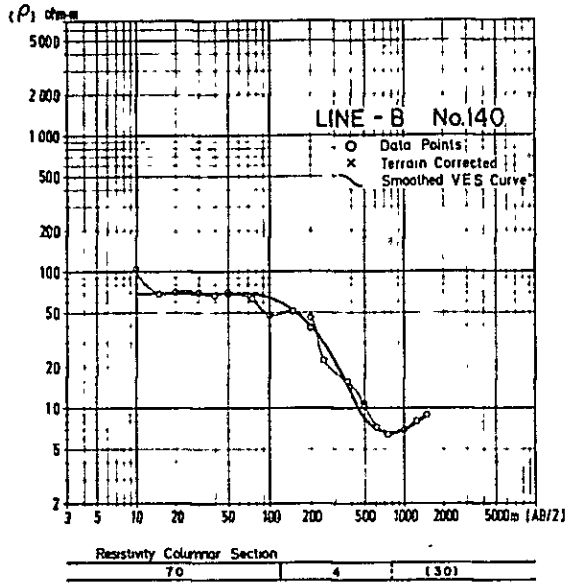
(ρ) ohm-m
LINE - B No.140
O Data Points
× Terrain Corrected
Smoothed VES Curve
5000
2000
1000
500
200
100
50
20
10
5
2
3 5 10 20 50 100 200 500 1000 2000 5000m (AB/2)
Resistivity Columnar Section
70
4
(30)

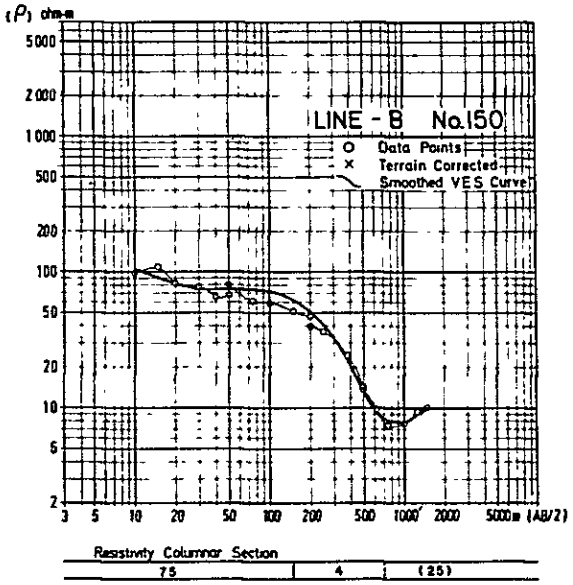
(ρ) ohm-m
LINE - B No.150
O Data Points
× Terrain Corrected
Smoothed VES Curve
5000
2000
1000
500
200
100
50
20
10
5
2
3 5 10 20 50 100 200 500 1000 2000 5000m (AB/2)
Resistivity Columnar Section
75
4
(25)

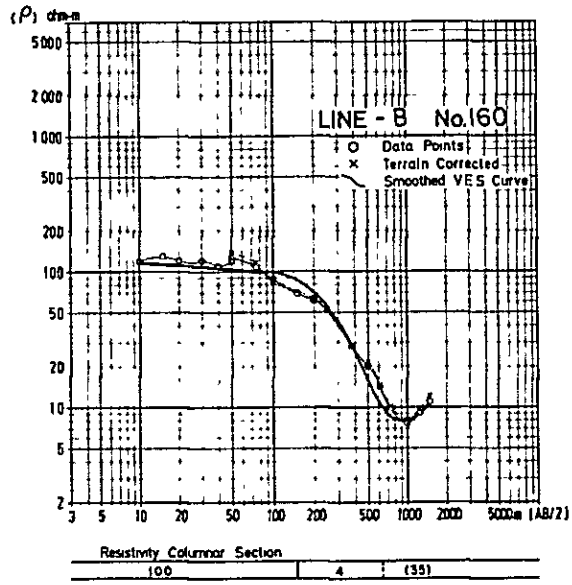
(ρ) ohm-m
LINE - B No.160
O Data Points
× Terrain Corrected
Smoothed VES Curve
5000
2000
1000
500
200
100
50
20
10
5
2
3 5 10 20 50 100 200 500 1000 2000 5000m (AB/2)
Resistivity Columnar Section
100
4
(35)

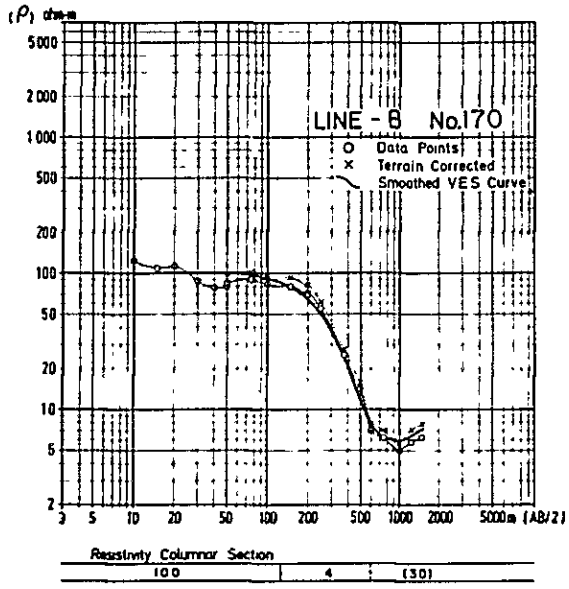
(ρ) ohm-m
LINE - B No.170
O Data Points
× Terrain Corrected
Smoothed VES Curve
5000
2000
1000
500
200
100
50
20
10
5
2
3 5 10 20 50 100 200 500 1000 2000 5000m (AB/2)
Resistivity Columnar Section
100 4 (30)

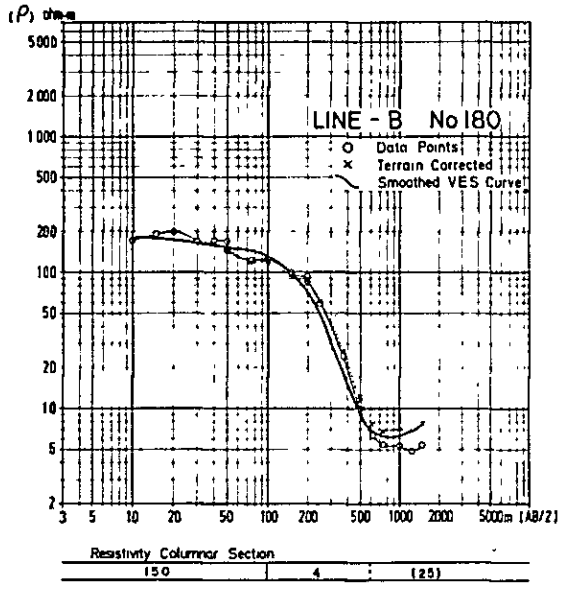
(ρ) ohm-m
LINE - B No.180
O Data Points
× Terrain Corrected
Smoothed VES Curve
5000
2000
1000
500
200
100
50
20
10
5
2
3 5 10 20 50 100 200 500 1000 2000 5000m (AB/2)
Resistivity Columnar Section
150 4 (25)

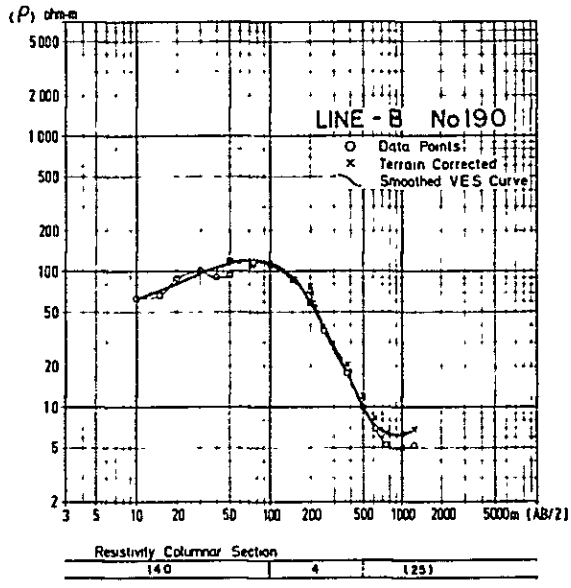
(ρ) ohm-m
LINE - B No.190
O Data Points
× Terrain Corrected
Smoothed VES Curve
5000
2000
1000
500
200
100
50
20
10
5
2
3 5 10 20 50 100 200 500 1000 2000 5000m (AB/2)
Resistivity Columnar Section
140 4 (25)

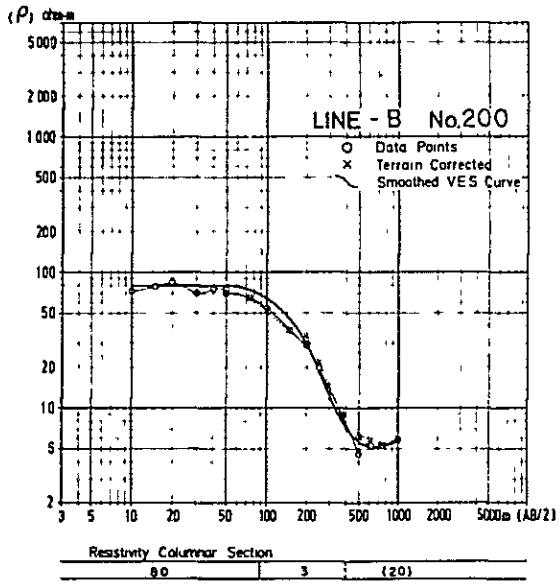
(ρ) ohm-m
LINE - B No.200
O Data Points
× Terrain Corrected
Smoothed VES Curve
5000
2000
1000
500
200
100
50
20
10
5
2
3 5 10 20 50 100 200 500 1000 2000 5000m (AB/2)
Resistivity Columnar Section
80 3 (20)

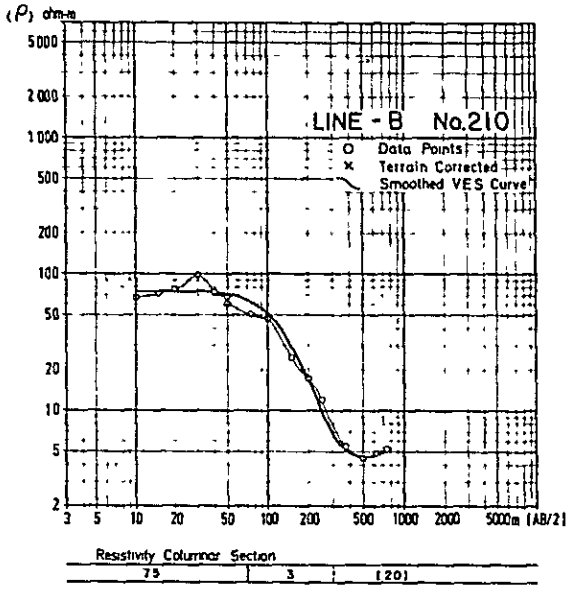
(ρ) ohm-m
LINE - B No.210
O Data Points
× Terrain Corrected
Smoothed VES Curve
5000
2000
1000
500
200
100
50
20
10
5
2
3 5 10 20 50 100 200 500 1000 2000 5000m (AB/2)
Resistivity Columnar Section
75
3
(20)

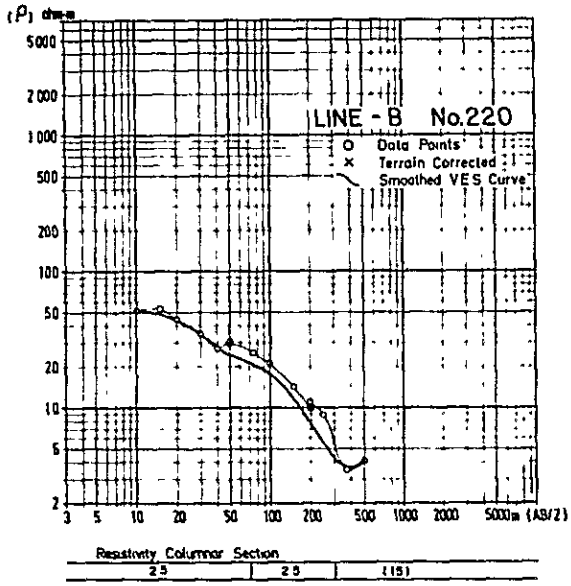
(ρ) ohm-m
LINE - B No.220
O Data Points
× Terrain Corrected
Smoothed VES Curve
5000
2000
1000
500
200
100
50
20
10
5
2
3 5 10 20 50 100 200 500 1000 2000 5000m (AB/2)
Resistivity Columnar Section
25
25
(15)

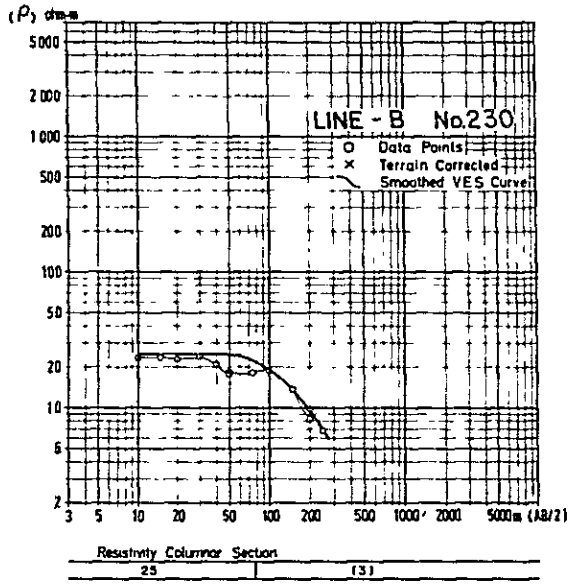
(ρ) ohm-m
LINE - B No.230
O Data Points
× Terrain Corrected
Smoothed VES Curve
5000
2000
1000
500
200
100
50
20
10
6
2
3 5 10 20 50 100 200 500 1000 2000 5000m (AB/2)
Resistivity Columnar Section
25
(3)